RESEARCH AND DEVELOPMENT TECHNICAL REPORT
ECOM-0059-F

OPTOELECTRONIC ELECTRON EMITTER

FINAL REPORT

BY

H. SCHADE
H. NELSON
H. KRESSEL
W. W. SIEKANOWICZ

MAY 1973

20080520255

DISTRIBUTION STATEMENT

ECOM

UNITED STATES ARMY ELECTRONICS COMMAND · FORT MONMOUTH, N.J.

CONTRACT DAAB07-71-C-0059
RCA LABORATORIES
PRINCETON, NEW JERSEY 08540

NOTICES

Disclaimers

The findings in this report are not to be construed as an official
Department of the Army position, unless so designated by other
authorized documents.

The citation of trade names and names of manufacturers in this report
is not to be construed as official Government indorsement or approval
of commercial products or services referenced herein.

Disposition

Destroy this report when it is no longer needed. Do not return it to
the originator.

OPTOELECTRONIC ELECTRON EMITTER

FINAL REPORT

21 OCTOBER 1970 TO 31 DECEMBER 1972

CONTRACT NO. DAAB07-71-C-0059   DA PROJECT NO. 7910217034401

ARPA Order No. 1686   Date of Contract: 10/21/70
ARPA Funding Program Code No. OD10   Amount of Contract: $125,965
USAECOM Funding No. 156-62703A05501 $24,970
Total Amount of Contract $150,935
Contract Expiration Date: 31 December 1972

DISTRIBUTION STATEMENT

Approved for public release; distribution unlimited

PREPARED BY

H. SCHADE, PRINCIPAL INVESTIGATOR (TEL. EXT.: 2910)
H. NELSON
H. KRESSEL, PROJECT SCIENTIST AND SUPERVISOR (TEL. EXT.: 2427)
W. W. SIEKANOWICZ

RCA LABORATORIES
TEL.: (609) 452-2700
PRINCETON, NEW JERSEY   08540

FOR

U. S. ARMY ELECTRONICS COMMAND, FORT MONMOUTH, NEW JERSEY   07703

FOREWORD

ABSTRACT

This report describes research performed during a two-year period in order to develop a semiconductor cold-cathode electron emitter with emission properties suitable for practical applications. Greatly improved cold-cathode structures based on negative electron affinity surfaces and on GaAs-(AlGa)As heterojunction structures grown by liquid phase epitaxy have been developed. The key to the successful development of this device was the ability to obtain highly doped p-type GaAs with electron-diffusion lengths as high as about 5 to 7 μm, and a technique for the confinement of the carrier flow to the desired emitting area.

Emission efficiencies (defined as the ratio of emission current/junction current) as high as 4.2% have been achieved under pulsed operation ($\sim$ 10% duty cycle), which represents an improvement by a factor of 35 since the start of this research program. Pulsed emission current densities as high as 7 A/cm^2 (1.7 mA total emission current) have been observed. These values are the highest ever reported for III-V compound semiconductor cold-cathodes based on negative-electron-affinity surfaces. Efficient dc operation has been reproducibly obtained with efficiencies as high as 1.9% and emission currents and current densities up to 190 μA and 0.4 A/cm^2, respectively.

A key property of the semiconductor cold-cathode, namely the energy distribution of the emitted electrons, has been measured for the first time. The half-width of the energy distribution of electrons, emitted from a GaAs-(AlGa)As structure, was found to be 160 meV which is distinctly narrower than that for a conventional thermionic cathode. The measured half-width is in fair agreement with calculations that take into account energy losses suffered by the electrons in the space charge region below the surface.

Extensive studies on dc operation and cathode life have been conducted under continuously pumped vacuum conditions as well as in sealed tubes, and operation was obtained for a period of 360 hr. No significant difference in cathode performance has been observed for these two ambient conditions. Shelf-life of cathode efficiency in sealed tubes has been measured to be essentially constant for a period of up to 5 months.

Some of the reasons for emission efficiency degradation have been determined. A major source for rapid degradation is electron-stimulated desorption from the collector electrode. Each of the following methods has been found to considerably reduce the rate of emission degradation:

1. Operation at sufficiently low collector voltages ($\lesssim$ 15 V), at which essentially no electron-stimulated desorption occurs.

2. Application of a magnetic field which separates the paths of electrons and ions and eliminates possible sputtering of the emitting surface.

3. Use of GaAs, instead of tungsten, as a clean collector material.

Finally, optoelectronic cold-cathodes instead of conventional thermionic cathodes have been incorporated into electron-beam-injected transistor (EBIT) tubes. It was shown that the activation procedures of the cathode did not adversely affect the performance of the EBIT targets. Their reverse current-voltage characteristics did not degrade, and the current gains ($\approx$ 1200 at 9 kV) and threshold beam voltages measured with electron beams from optoelectronic cathodes were essentially identical to those obtained from conventional oxide and thoria cathodes.

Compared with conventional thermionic cathodes, the semiconductor cold-cathodes developed in this program offer the following advantages:

1. Instantaneous operation, since no cathode heating is required.

2. Simplicity in pulsed operation by pulsing the junction current without the need for an additional modulating grid.

3. Lower noise due to a narrower energy distribution of the emitted electrons.

4. Lower power requirements to provide electron emission.

However, the problem of cathode life requires further investigations. Although there is practically no efficiency degradation during periods of nonoperation, relatively slow degradation persists, even under optimum conditions in exploratory test tubes. While the mechanism for this slow degradation needs to be explored by basic surface research on the emitting surface, the cathode life in practical tubes, such as the EBIT tube, is expected to be significantly improved by more elaborate tube engineering involving improved electron beam optics and possibly ion trapping.

TABLE OF CONTENTS

LIST OF ILLUSTRATIONS

LIST OF ILLUSTRATIONS (Continued)

LIST OF TABLES

I. INTRODUCTION

The development of semiconductor cold-cathode emitters suitable for vacuum-tube applications has been motivated by the need for emitters that have narrower electron-velocity distributions than present hot-cathodes (for better focusing of the electron beam), can be readily modulated, are capable fo being fabricated in array form, have long life, and do not require the heat shielding which complicates tube construction.

The present research program concentrated on GaAs p-n junction structures which rely on negative-electron-affinity surfaces[1] to obtain high electron-emission efficiency (defined as the ratio of emission current/diode current) at room temperature. This surface allows electron escape probabilities in excess of 10% at room temperature. The electrons to be emitted can be generated either by direct injection into the surface region or by first generating light (electroluminescence) which is absorbed in a p-type surface layer that acts as a photoemitter. Devices involving the latter characteristic are called opto-electronic cold-cathodes[2]; they avoid current constriction in the vicinity of the ohmic contact to the emitting surface, which is frequently a major problem in cold-cathodes utilizing direct electron injection. Devices of the direct-injection type, however, do have potential applications as small-area high-current-density emitters.

The objective of this contract was to determine the feasibility of an optoelectronic electron emitter operating at a current efficiency of at least 1% and at an emission current density of $\gtrsim$ 100 mA/cm^2. The program was based on the previous encouraging performance at RCA Laboratories of a structure that consisted of a silicon-compensated (AlGa)As electroluminescent diode covered with an absorbing p-type GaAs:Zn layer having a negative-electron-affinity surface. An efficiency of 0.11% at an emission current density of 1 mA/cm^2 had been achieved[2] under conditions which were known to be far from optimum. Based on these initial results, the objective of the present contract was planned to be reached with the following program:

(1) Optimization of the various structural parameters of the device such as doping, electron-diffusion length, layer thicknesses, contacting, and surface activation, - all in order to achieve at least the required efficiencies and emission-current densities.

(2) Life testing under dc conditions at varying anode voltages. In particular, it is of interest to determine whether cold-cathode operation is feasible with anode voltages of several thousand volts, a requirement for some applications, such as the electron-beam-injected transistor (EBIT).

1

II. PRINCIPLE OF SEMICONDUCTOR COLD-CATHODE OPERATION

The basic elements of a semiconductor cold-cathode are a p-n junction and a low-work-function surface on the p-side. The p-n junction is used to inject electrons into the surface region of the p-side, from where, due to the low work function, efficient electron emission into the vacuum can occur at room temperature. Figure 1 illustrates the simplest case of cold-cathode operation in the band scheme of a device operating with *direct* electron injection.
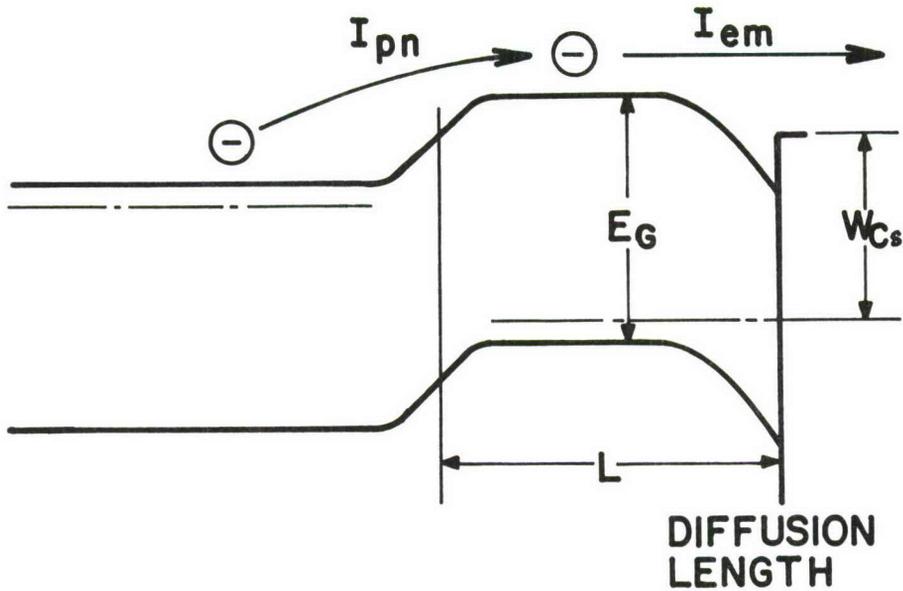
Figure 1.   Energy-band scheme for a semiconductor cold-cathode operating by direct electron injection into the region of a negative-electron-affinity surface. For negative electron affinity the work function W_{Cs} is smaller than the bandgap E_G.

The key to any efficient cold-cathode emission is the attainment of a negative-electron-affinity surface, meaning that the work function is lower than the bandgap of the material (see Fig. 1). Under such a condition, the electrons injected into the conduction band of the p-side need no additional energy in order to be emitted into vacuum. However, they must be injected to within about one electron-diffusion length from the emitting surface; otherwise, they recombine before being emitted. Hence, a necessary condition for efficient electron emission from a direct-injection-type structure is that the p-n junction must be located less than a diffusion length L from the emitting surface, i.e., the thickness of the p-layer is required to be

$$d \le L \tag{1}$$

With L being on the order of micrometers, the current spreading under the contact to the thin p-layer is rather limited, and, therefore, electron emission can occur only over relatively small emitting areas ($\lesssim 5 \times 10^{-4}$ cm^2) on the p-layer surface.

A modified scheme of a semiconductor cold-cathode which essentially eliminates problems of current constriction under the contact to the emitting surface is shown in Fig. 2. This so-called optoelectronic cold-cathode structure
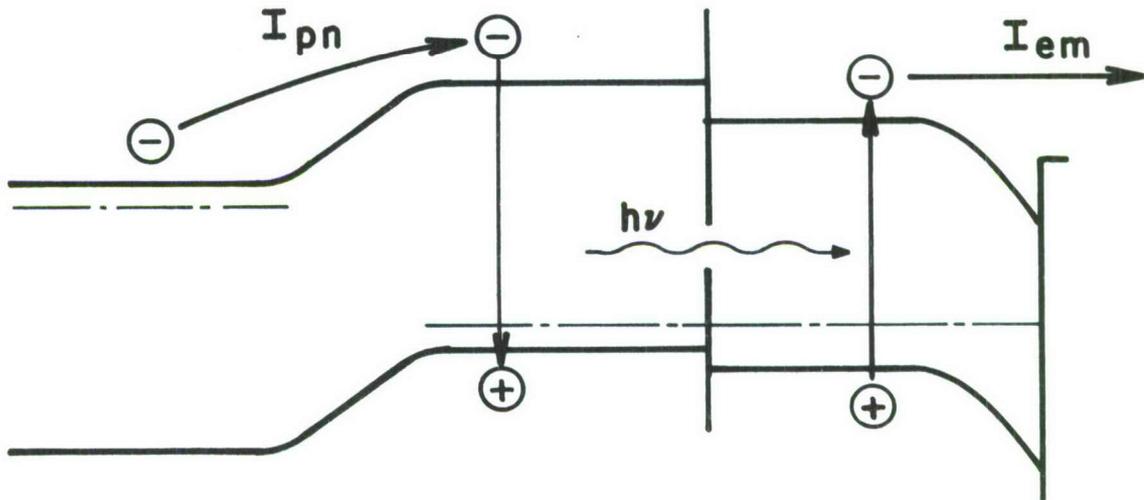
Figure 2. Energy-band scheme of an optoelectronic semiconductor cold-cathode.

consists of an electroluminescent diode of higher bandgap material, (AlGa)As:Si, covered with a thin top layer of lower bandgap material, GaAs:Ge, whose surface is activated to a condition of negative electron affinity. Electron emission from such a structure is obtained as follows.

Under forward bias, electrons are injected into the p-type (AlGa)As region where they recombine radiatively. The emitted photons ($h\nu$ = 1.41 - 1.6 eV) are strongly absorbed in the highly p-type GaAs surface layer (E_g = 1.42 eV), thus creating electron-hole pairs. A substantial number of the electrons that diffuse to the surface are then emitted into vacuum, provided the surface has been activated to a condition of negative electron affinity. In this structure, current constriction is minimized, since current spreading can extend not only over the thin p-type GaAs layer but also over the much thicker p-type (AlGa)As layer. Thus, current flow, light generation, and absorption, and hence also electron emission, are fairly homogeneously distributed over the p-layers, allowing the fabrication of large-area emitters.

Next, we consider the diode factors which influence the emission efficiency. Theoretically, the optoelectronic structure can be treated as a back-illuminated Ge-doped GaAs photocathode[3]. For surfaces having a negative electron affinity, the concentration of electrons available for emission can

3

be calculated with a diffusion model[4]. The basic equation involving the electron concentration n as a function of the distance z from the semiconductor surface is

$$- D \frac{\partial^2 n}{\partial z^2} + \frac{n}{\tau} = G \tag{2}$$

where D is the electron diffusion constant, τ the electron life time, and G the generation rate for electrons. For the back-illuminated photocathode, the generation rate is given by

$$G = I(1-R')\{\exp[-\alpha(d-z)] + R \exp[-\alpha(d+z)]\} \tag{3}$$

where I is the photon-flux incident from the (AlGa)Ga electroluminescent diode onto the GaAs layer, α is the absorption constant, d is the thickness of the GaAs layer, R' is an effective reflectivity which combines the effects of reflection at the (AlGa)As-GaAs heterojunction and at the GaAs-vacuum interface, and R is the reflectivity of the GaAs-vacuum interface.

Combination of Eqs. (2) and (3) and a suitable choice of boundary conditions lead to an expression for the electron-emission efficiency. Assuming no recombination at the (AlGa)As-GaAs interface ($\partial n/\partial z = 0$ at z = d) and infinite recombination velocity at the GaAs surface (n = 0 at z = 0), one obtains for the emission efficiency[3]

$$\eta = \eta_i P(1-R) \left\{ \frac{1 - [\cosh(d/L)+(\alpha L)^{-1} \sinh(d/L)] \exp(-\alpha d)}{\cosh(d/L) [1 - (\alpha L)^{-2}]} \right\}$$

$$+ \eta_i PR \exp(-\alpha d) \left\{ 1 - \left[\frac{\cosh(d/L) - \alpha L \sinh(d/L)+(\alpha L)^2 \exp(-\alpha d)}{\cosh(d/L)[1-(\alpha L)^2]} \right] \right\} \tag{4}$$

where η_i is the internal quantum efficiency of the (AlGa)As electroluminescent diode, P is the electron escape probability at the GaAs surface, d is the thickness of the GaAs layer, L is the electron diffusion length, and α is the absorption constant of GaAs for light generated in the electroluminescent diode.

Thus, having stated the actual theoretical problem we now proceed with approximations for the main parameters which determine the optoelectronic cold-cathode performance. The emission efficiency for the structure shown in Fig. 2 depends on the following factors: (1) the internal quantum efficiency of the (AlGa)As electroluminescent diode; (2) the relationship between the electron-diffusion length, thickness, and optical absorption constant of the GaAs layer;

4

and (3) the escape probability of the photoexcited electrons from the GaAs surface. A necessary condition for optimum use of all available photons is

$$L > d > 2/\alpha \qquad (5)$$

where $2/\alpha$ is the distance over which about 90% of the photons are absorbed ($\alpha = 1 \times 10^4$ cm^{-1} is the GaAs absorption constant at $h\nu \cong 1.5$ eV). Provided Eq. (5) is satisfied the emission efficiency η is roughly determined by η_i, and the electron escape probability P at the GaAs surface:

$$\eta \cong \frac{1}{2} \eta_i P \qquad (6)$$

The factor 1/2 reflects the fact that only about half of the photons are available for absorption in the top GaAs layer, the other half being absorbed in the base region of the diode. The internal quantum efficiency is known to be at least 50%. The realized value of P is estimated from our previous data[5] to be 10 to 15%. Using these numerical estimates, the calculated optoelectronic cold-cathode efficiency is 3 to 4% with no further improvements in surface activation. However, since P can be as high as 30 to 50%[6], the potential optoelectronic cold-cathode efficiency is approximately 10%.

The direct-injection-type structure shown in Fig. 1 theoretically allows a higher emission efficiency, since no losses due to photon coupling are involved. Provided that Eq. (1) holds and that no severe current constriction under the contact to the emitting surface occurs, the emission efficiency may approach the surface escape probability and thus be a factor 2 to 4 higher as compared with that of optoelectronic structures. By using a GaAs-(AlGa)As p-n heterojunction where the GaAs:Ge layer is doped to a level of 5×10^{17} to 10^{18} cm^{-3} it is possible to ensure nearly perfect electron injection as well as an electron diffusion length of at least 5 μm. With this type of device, assuming a surface escape probability of 10 to 15%, the predicted emission efficiency should therefore reach about 10%, with higher values ($\sim$ 30%) possible if the escape probability reaches the maximum possible value.

Although the bulk of our work was concentrated on the optoelectronic device, a number of the direct-injection devices were also studied. Both types are fabricated by an identical materials technology.

III. DEVICE DESCRIPTION

The devices used here differ from those described previously[2] in that they were prepared solely by liquid-phase epitaxy. For the optoelectronic cold-cathode structure as shown in Fig. 3, the electroluminescent diode emission peaked at 8700 to 8800 Å. A thick (10 to 13 μm) GaAs:Ge layer was used
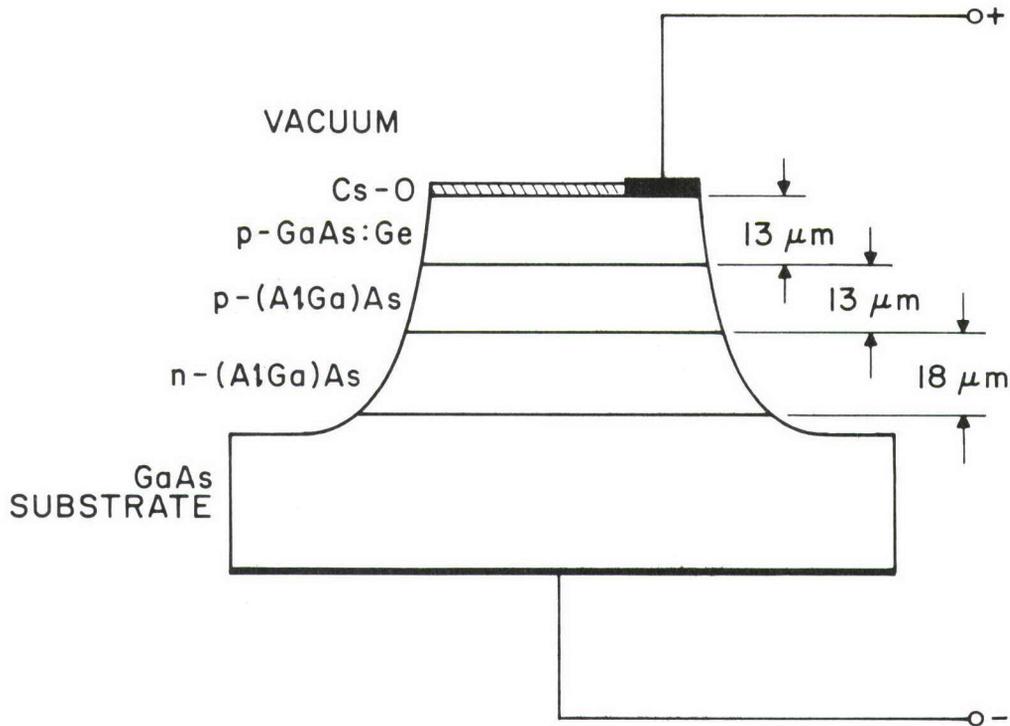
Figure 3. Schematic of optoelectronic cold-cathode structure.

with a hole concentration of about 5×10^{17} cm^{-3} in place of the previous thin (about 1 μm) Zn-doped layer with a concentration of about 1×10^{19} cm^{-3} prepared by vapor-phase epitaxy. GaAs:Ge layers were used because their electron-diffusion lengths had been previously found by us[5] to be typically between 5 and 7 μm. The thick p-type region is desirable to more fully absorb the light emitted by the (AlGa)As diode and to minimize current constriction under the ohmic contact.

A major requirement for practical cold-cathodes are emitting areas of a desired geometry to obtain small emitting areas for cathode arrays and to prevent the flow of "wasted" current through the diode. Therefore, a novel cathode structure in which electron injection and emission is confined to a specific area controlled with regard to size and locus was used. This structure comprises a back-biased junction over part of the device surface confining the forward current flow to a small emitting area. A cross section of the optoelectronic version is shown in Fig. 4. The materials, thicknesses, and the

6

VACUUM   EMITTING
                          AREA

Cs - O
p- Ga As : Ge
p -(Al Ga)As : Si
n -(Al Ga)As : Si
p- Ga As : Zn

Ga As
SUBSTRATE
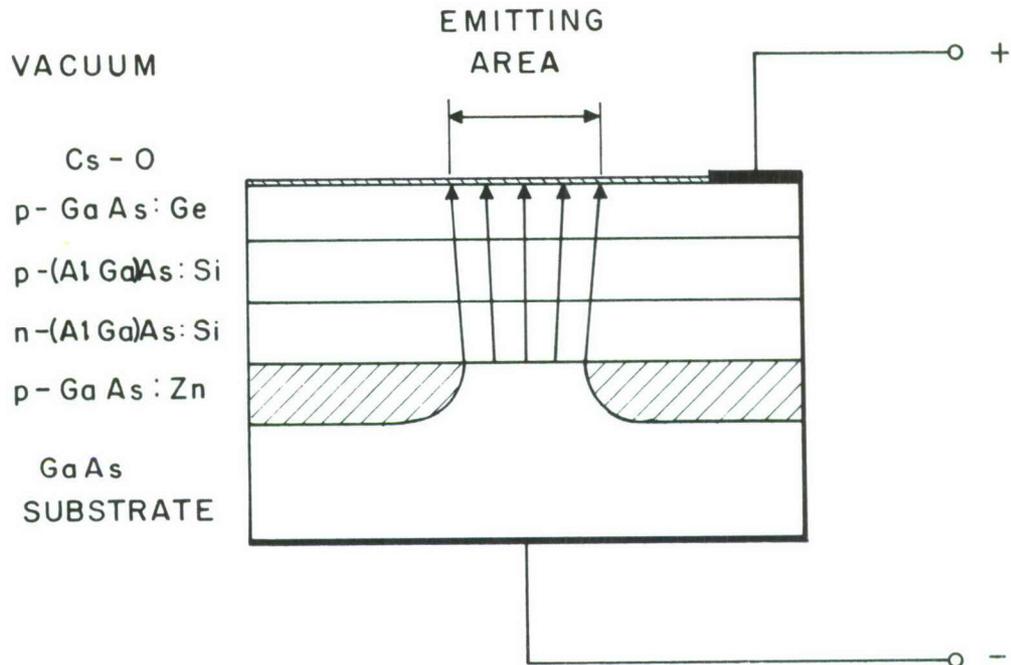
Figure 4. Optoelectronic cold-cathode structure providing for
           confinement of electron emission by a Zn-diffused
           partial layer forming an "aperture" in the n-type
           substrate.

sequence of the layers are similar to the structure shown in Fig. 3, except
that an additional p-layer is introduced by Zn diffusion into the n-type sub-
strate, forming an n-type "aperture." Thus, by using masking techniques, the
desired sizes and locations of the emitting area can be delineated prior to
epitaxial growth, and electron injection across the p-n junction (and hence
electron emission) is substantially confined to the area above the "aperture."

The direct-injection version of the confinement structure, shown in Fig. 5,
is designed for applications where the emitting area can be smaller. Here the
electrons are injected from the (AlGa)As n-region directly into the GaAs:Ge
p-region. The heterojunction improves the electron-injection efficiency. In
the process of growing the GaAs:Ge p-layer, a gradient is introduced in the
doping concentration such that the hole concentration near the surface is
higher than at the heterojunction interface. Some of the electrons reach the
surface directly, while others recombine radiatively near the junction and
some of the photons are then reabsorbed near the surface to create hole-elec-
tron pairs. Note that the structure shown in Fig. 5 contains an "aperture"
as discussed above, and thus provides for confinement of electron emission.

The optoelectronic cathode emitting areas studied ranged from 2×10^{-4}
to 1×10^{-2} cm^2 with no obvious dependence on the area, while those of direct-
injection cathodes ought not to exceed 5×10^{-4} cm^2 to assure reasonable cur-
rent spreading.

7

VACUUM

EMITTING
AREA

○ +

Cs – O

p – GaAs: Ge

4 μm

n – (AlGa)As

6 μm

p – GaAs: Zn

Ga As
SUBSTRATE

○ –
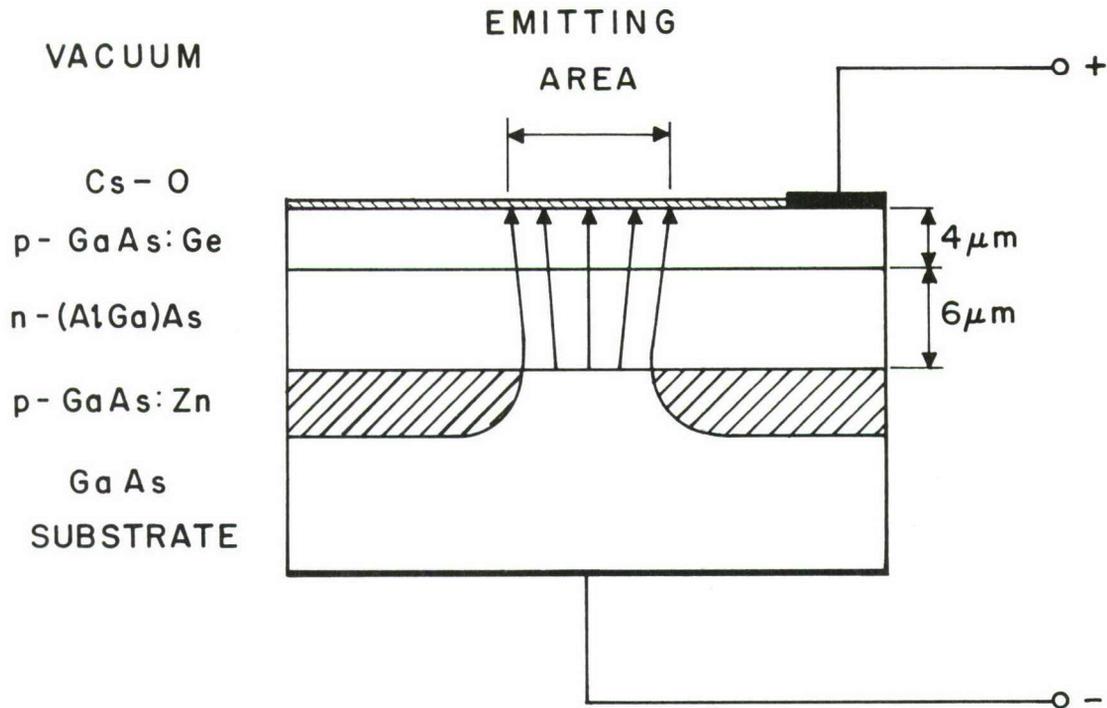
Figure 5.   Cold-cathode structure providing direct electron
injection from an "aperture" and hence confined
electron emission.

Ohmic contact to the n-side of the junction was made by indium, while a
point contact was applied to the p-side. In both confinement structures, the
contact to the cathode surface can be made remote from the emitting area, and
thus the surface lead connection does not interfere with the emission of elec-
trons into the vacuum. However, it is still important to make the p-type
region as conductive as possible to prevent current constriction in the periph-
ery of the emitting area which would result in nonuniform electron emission.

IV. DEVICE FABRICATION

Cold-cathode structures as described in Section III are prepared from epitaxial material grown by the liquid-phase process using a graphite boat as shown in the cross section of Fig. 6[7]. An n-type GaAs substrate of <100> orientation is placed in a recessed area R of a graphite slide S. A melt composed of Ga, Al, Si, and GaAs is placed in bin B_1, and another melt composed
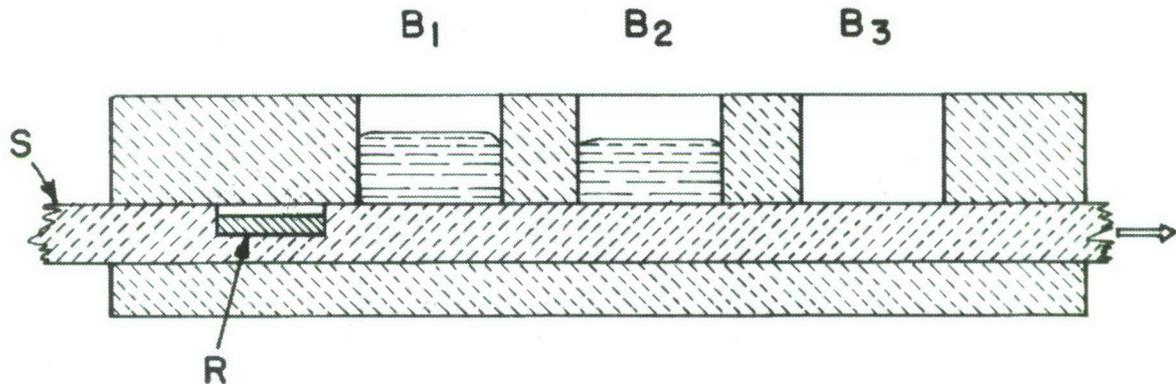
Figure 6. Graphite boat used in growth of optoelectronic cathode material.

of Ga, Ge, and GaAs is placed in bin B_2 of the graphite boat. The boat is inserted in a quartz furnace tube and heated in a flow of pure hydrogen to a maximum temperature of about 875°C. The graphite slide is then pulled into a position such that the substrate in the recessed area R forms the bottom of bin B_1. As the furnace is allowed to cool to a temperature of about 810°C, a Si-doped epitaxial (AlGa)As layer, the first portion of which is n-type and the final portion p-type, is grown onto the surface of the GaAs substrate[8]. The graphite slide is then pulled into the position where the substrate forms the bottom of bin B_2. Upon further cooling to about 750°C, precipitation from the melt in this bin results in the growth of a Ge-doped, p-type GaAs surface layer. The processed substrate is then pulled into the empty bin B_3, and the furnace is allowed to cool to a temperature at which the graphite boat can be removed from the furnace. A photomicrograph of a cross section of a portion of a cold-cathode wafer, prepared as described above, is shown in Fig. 7.

It is not necessary to adjust the growth cycle to exactly control the layer thickness, since we found that chemically polished surfaces (bromine in methanol) could be reproducibly activated to photosensitivities in excess of 800 μA/1m. Thus, the Ge-doped surface layer can be thinned to the desired value after growth, normally to about 10 μm by lapping and polishing. Thereafter, cold-cathode structures as shown in Figs. 3 to 5 are fabricated from the processed wafer by masking and etching techniques.
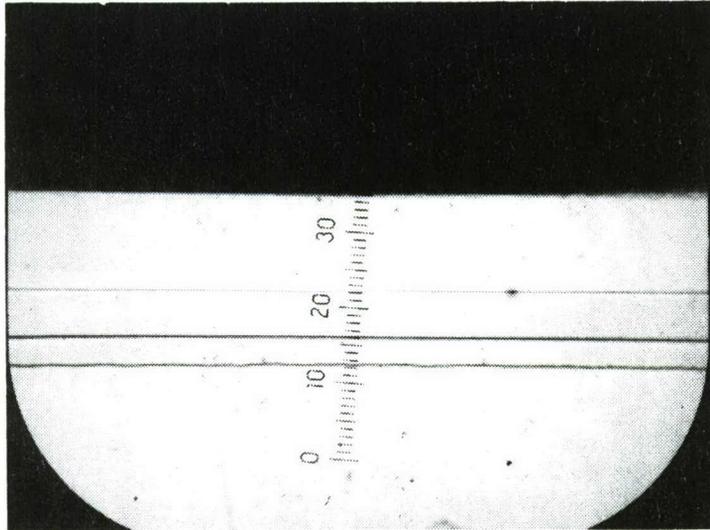
Figure 7. Photomicrograph showing a cross section of
optoelectronic cathode material.

Numerous cold-cathode wafers of the type described above were prepared in
the course of work directed toward the determination of doping concentrations,
doping gradients, and geometrical parameters which lead to optimum cold-cathode
efficiency.

V. EXPERIMENTAL TECHNIQUES

To obtain cold-cathode emission, the devices were heat-cleaned in vacuum (base pressure below 1×10^{-9} Torr) by electron bombardment for several minutes at temperatures close to the decomposition temperature of GaAs. The GaAs surface was then activated with conventional cesium-oxygen treatments to a state of negative electron affinity. Cesium was provided by heating cesium chromate in a tantalum channel, and oxygen was leaked into the vacuum changer by heating an attached silver tube. The activation process was monitored by measuring the white-light photoemission from the GaAs top surface. Typically, photosensitivities between 700 and 1000 μA/lm were obtained.
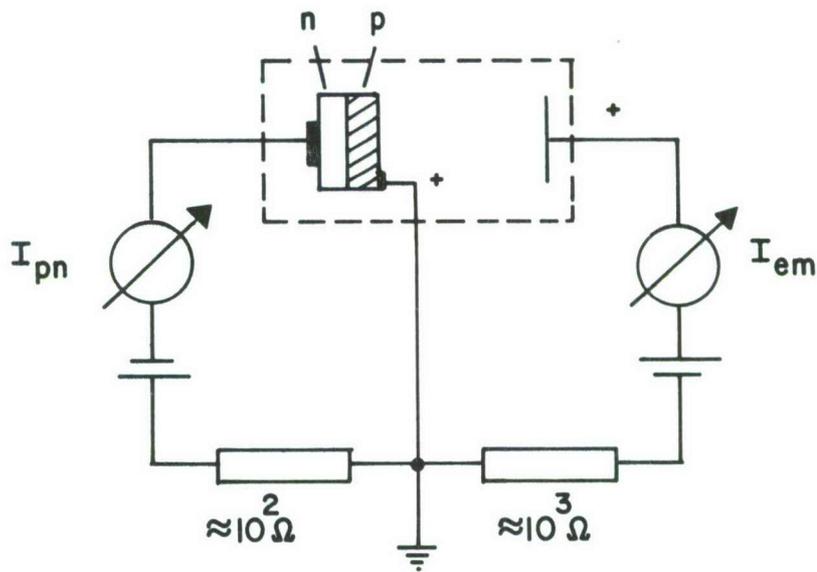
Figure 8. Circuit configuration used to measure cold-cathode emission. The emission efficiency is defined as $\eta = I_{em}/I_{pn}$.

Upon reaching maximum photosensitivity, cold-cathode emission was measured using the circuit shown in Fig. 8. Two different modes of operation were applied:

(1) In the pulsed mode 10- to 100-μsec pulses (0.1 to 10% duty cycle) are applied to the electroluminescent diode, and the emission current is collected with anode voltages as high as 2500 V. This mode of operation avoids heating of the sample as well as space-charge limitation of the emission current. Thus, the full capabilities of the device structure can be tested.

(2) In dc operation, forward currents of about 10^2 A/cm^2 can be drawn through the p-n junction without significant heating of the structure. At the same time, precautions are taken (see below) in order to eliminate possible damage to the emitting surface.

11

Because of the flexibility required for systematic studies of the emission properties, part of the program was conducted in continuously pumped vacuum tubes. Upon reaching emission properties of practical interest, however, provisions were also made to prepare sealed tubes, which are required in potential applications. Initially, glass-sealing the tube from the vacuum system resulted in a loss of the surface activation of the sample, due to the release of impurities from the glass constriction. This difficulty was over-come by using a copper constriction which could be pinched off without causing a significant loss in surface activation. The experimental tube usually was pinched off, after the surface activation had remained stable for at least 12 hours under continuous pumping.

VI. EXPERIMENTAL RESULTS

Though at the beginning of the contract period, the best performance reported for semiconductor cold-cathodes[2] was an emission efficiency of 0.11% at an emission-current density of 0.001 A/cm^2, the goals of the present contract were set for cold-cathodes to exhibit a minimum efficiency of 1% and a minimum emission-current density of 0.1 A/cm^2. As we will show below, these goals were substantially exceeded during the course of this work. The emission data obtained here were the highest values ever reported for any III-V compound semiconductor cold-cathode.

A. PULSED OPERATION

Figure 9 shows the emitted current as a function of the pulsed diode current (7% duty cycle) of a sample yielding an emission efficiency of 4.1% and a total emission current of 800 µA. This sample had a structure similar to the
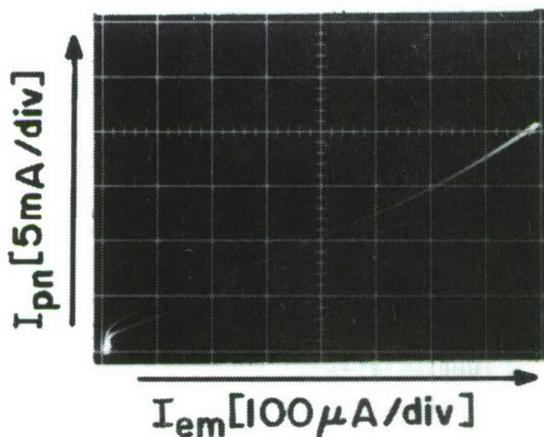
$$\eta = I_{em}/I_{pn} = 4\%$$

Figure 9. Emitted current as a function of the pulsed
           junction current of a cold-cathode using
           direct injection.

one shown in Fig. 5. The emitting area was estimated to be approximately 1.7×10^{-4} cm^2, and accordingly the current density of electron emission reached nearly 5 A/cm^2. For a different sample of the optoelectronic type shown in Fig. 4, emission-current densities as high as 7 A/cm^2 (1.7 mA total emission) were obtained at an efficiency of 1.1%, while at 3.2 A/cm^2 the efficiency was

1.7%. The latter case is shown in Fig. 10. During the course of work directed toward the determination of optimum surface activation procedures and of optimum structural device properties, such as doping concentrations, doping gradients,
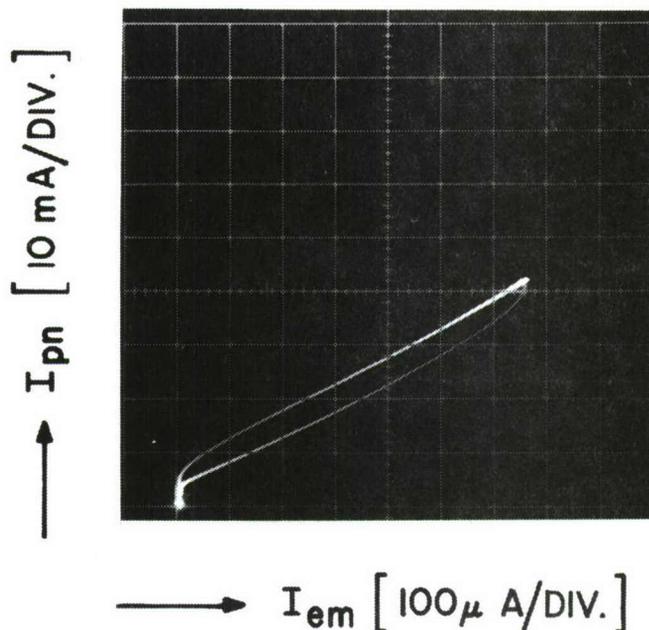
Figure 10. Emitted current as a function of the pulsed junction current of an optoelectronic cold-cathode with an overall efficiency of 1.6%. Note that because of diode leakage emission does not start at zero junction current; the differential efficiency, 1.74%, is therefore higher than the overall efficiency.

and layer thicknesses, we have tested 18 samples. Of these examples, ten were of the optoelectronic type and eight of the direct-injection type. The following table shows the number of samples yielding emission efficiencies above certain limits.

TABLE I

Emission Efficiencies

Type	>2%	>1%	>0.4%	>0.1%
Optoelectronic Structures		2	6	3
Direct-injection Structures	4	3	1	

14

As one might expect from the theoretical discussion (see p. 5), the efficiencies of the direct-injection cold-cathodes were higher. However, in both cases the highest values obtained are still below the maximum possible efficiencies. Moreover, the total number of samples it too small to draw the conclusion from Table I that the efficiencies of optoelectronic cold-cathodes are generally lower.

The samples accounted for in Table I were all processed in exploratory vacuum diode tubes. In addition, we have processed several samples in advanced exploratory tubes, such as electron-beam injected transistor (EBIT) tubes (see p. 28) or vidicon tubes. The latter were chosen as readily available test vehicles in order to investigate activation procedures in the presence of a commonly used electron gun. The maximum efficiencies achieved in these advanced tubes typically did not exceed 0.2% because adequate in situ heat-cleaning of all metal parts, such as the electron gun structures, could not be provided. This is thought to adversely affect the cleanliness of the cold-cathode surface prior to activation.

B. DC OPERATION, CATHODE-LIFE, AND MECHANISMS OF EFFICIENCY DEGRADATION

1. Operation in Continuously Pumped Tubes

Thus far, we have described the maximum initial emission efficiencies and currents which were achieved in optimizing structural parameters of the device. If certain precautions are not taken in operating negative-electron-affinity cathodes, however, the emission efficiency decreases with time during operation, as exemplified in Fig. 11.

This efficiency degradation is caused by a change in the surface condition. In studying such changes it ought to be noted that the activated surface is of a very delicate nature, comprising only a few monolayers of cesium and oxygen on an atomically clean surface. Thus, it is not surprising that the loss or addition of monolayer amounts can be harmful.

Several experiments were aimed at determining the conditions for stable dc emission from cold-cathodes.

The following factors may result in emission efficiency degradation due to changes in the activation of the emitting surface: (1) adsorption of residual gases; (2) desorption of cesium and/or oxygen; (3) ion bombardment of the emitting surface due to impact ionization of residual gas atoms by the emitted electrons; (4) passage of high emission-current densities through the cesiated surface; and (5) ion bombardment or sputtering of the emitting surface due to electron-stimulated desorption of ions or neutrals from the collector electrode.

The first two mechanisms would cause degradation even during periods when the cathode is not operated. We have found, however, that the activated cathodes do have an excellent "shelf life." Thus, the surface activation stays essentially constant over extended periods of time during which the emission efficiency has been checked occasionally. This has been found for samples in
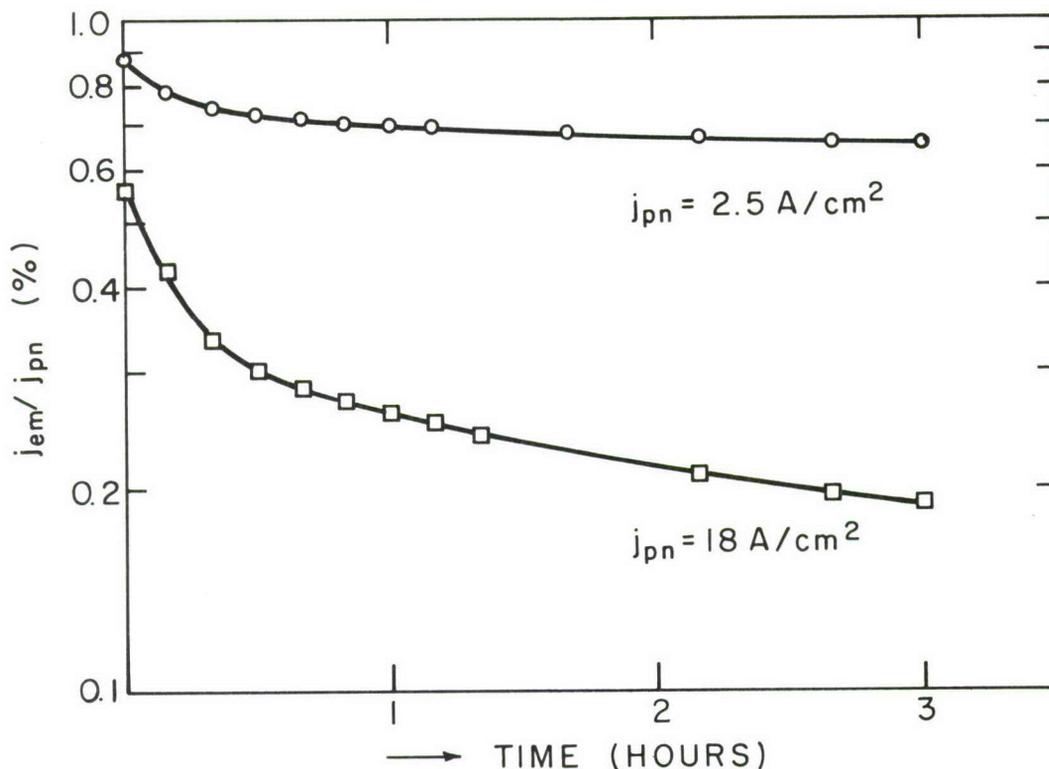
Figure 11.   Emission efficiency as a function of time during
             pulsed operation (0.1% duty cycle).

continuously pumped tubes as well as in sealed tubes. For example, the emission efficiency of a sample in a sealed tube stayed practically constant (2.0 to 1.9%) over a period of two months. (For continuous cathode operation in sealed tubes see p. 20.)

We have found that the efficiency degradation occurs only during *operation* and hence must be caused by processes involving the emitted electrons. Factors (3) to (5) listed above constitute operation-induced mechanisms. However, we can further eliminate the third mechanism (3) since the degradation rates were not affected by a change in vacuum from 5×10^{-10} to 1×10^{-8} Torr.

With regard to the fourth mechanism (4), there is yet insufficient information to appraise its contribution to the emission degradation observed. There is evidence, however, that the passing of electrons through the activated surface is not a cause of *rapid* degradation.

Our experiments show that a major source of rapid efficiency degradation is the fifth mechanism in which impurities are desorbed from the collector electrode by the impinging electrons ("electron-stimulated desorption"). These impurities are in part readsorbed on the emitting surface and are thus responsible for a deterioration of the surface activation. In this connection, we

16

have demonstrated that efficient, dc cold-cathode operation can be greatly extended by one of three procedures: (1) collection of the emitted electrons at sufficiently low anode voltages; (2) application of an additional magnetic field in order to separate the paths of electrons and ions and to eliminate possible sputtering of the emitting surface; and (3) use of a clean semiconductor anode.

Electron-stimulated desorption from metals typically occurs only for electron energies higher than about 20 V[9]. Thus, when a cold-cathode was operated with a collector voltage of 15 V and an emission current of 30 μA dc for over 50 hours the emission efficiency decreased only from 0.16 to 0.15% (see Fig. 12). A similar structure with an emitting area of $\sim 2 \times 10^{-4}$ cm^2 operated at 30 V and at a total emission current of 80 μA dc (emission-current density 0.4 A/cm^2) for 8 hours (at which point the test was terminated), at a constant efficiency of 0.43%. From these measurements it can also be concluded that, at least for current densities studied thus far, the process of emission itself, i.e., the transport of electrons across the activated surface, is not a cause of rapid degradation.
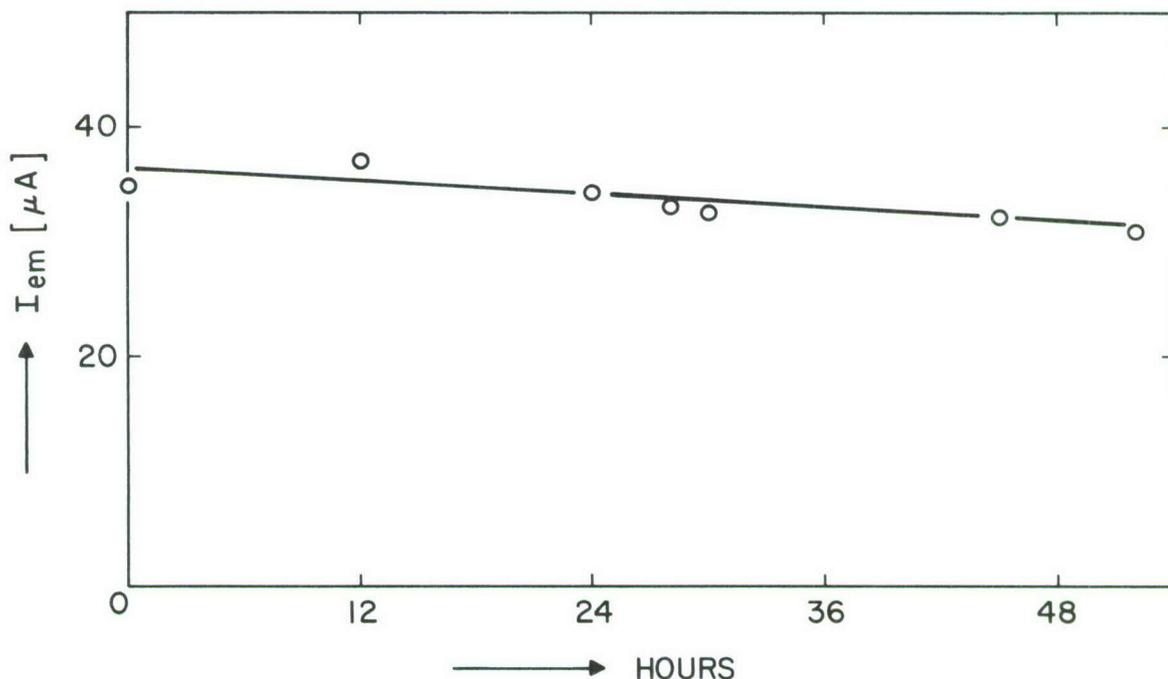
Figure 12. DC operation of a cold-cathode at an anode voltage of 15 V.

At higher collector voltages (about 50 V) dc cold-cathode operation tends to deteriorate markedly, and Fig. 13 clearly illustrates that the rate of decrease in emission depends on the state of the collector. Here, the emission current has been collected in a close-proximity geometry by a planar anode which could be moved parallel to the emitting surface. Moving of the anode
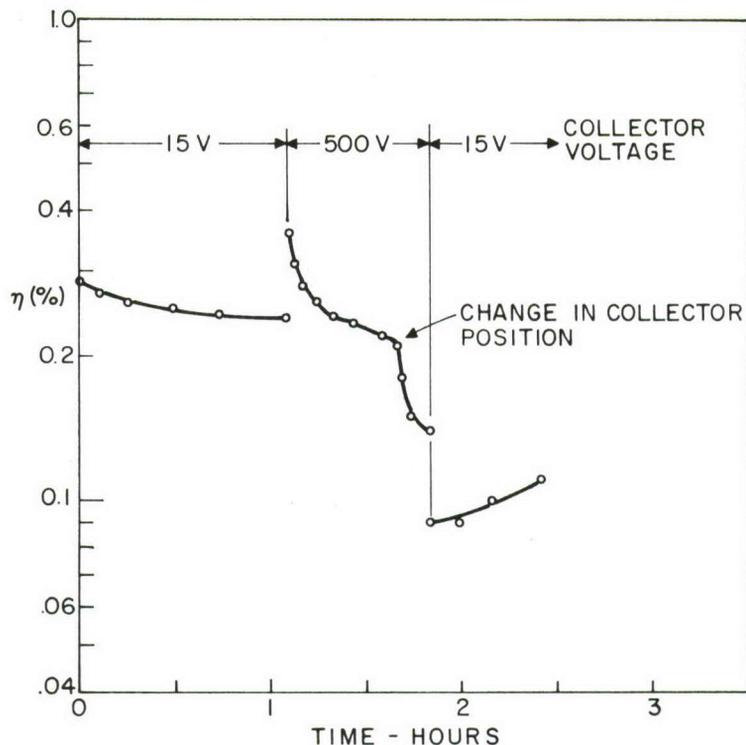
Figure 13. DC operation of a cold-cathode at anode voltages
of 15 and 500 V. The rise in efficiency shown
after 2 hours is due to the mechanism explained
in Section VI.C.

into a new position exposes a new area of the anode to the electron beam and
as a result, the rate of efficiency degradation is increased. It is thought
that this increase results from a higher desorption rate of the collector
area which has not been "cleaned" by impinging electrons. The desorbed species
are readsorbed on the emitting surface in close proximity to the collector,
and thus give rise to a deterioration in surface activation.

The amount of ions and neutrals striking the emitting surface can be
greatly reduced if in addition to the electric field a magnetic field is
applied. Thus, the paths of electrons and ions are different, and the elec-
trons are collected at a larger distance from the emitting surface. Using a
crossed-field geometry[10], a magnetic field of 100 G was sufficient as long
as the collector voltage was not more than 300 V. The magnetic field was
produced by Helmholtz coils and applied externally to the vacuum chamber.
Figure 14 clearly demonstrates the effect of a magnetic field on dc operation
of a cold-cathode sample at 300 V. The explanation for the behavior shown is
similar to that in Fig. 13. While in the previous experiment the collector
was moved relative to the electron beam, here the electron beam has been moved
relative to the collector. In both cases, the electrons are collected by an
anode area not previously "cleaned" by the impinging electrons, and in the
latter case, also moved closer to the emitting surface.

18
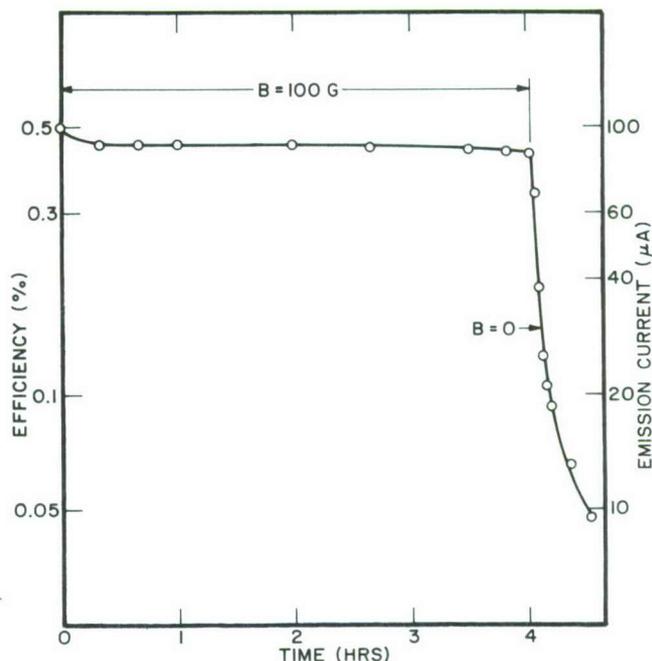
Figure 14. DC operation of a cold-cathode at an anode voltage of 300 V showing the effect of an additional magnetic field perpendicular to the electric field.

Another cold-cathode sample was operated at 300 V and, with a magnetic field applied, no degradation was observed during 4 hours at 85 µA dc total emission, and during the next 20 hours, the emission efficiency dropped only from 0.42 to 0.32%. Upon removing the magnetic field, however, the emission efficiency dropped by a factor of 4 in only 5 minutes.

Since we have clearly established that a major source of cold-cathode degradation is electron-stimulated desorption from the collector, we investigated the possibility of using a semiconductor (GaAs) instead of a metal as anode material. Semiconductor surfaces can be made atomically clean at considerably lower temperatures as compared with metals used in vacuum technology. Furthermore, the sticking probabilities for readsorption on cleaned semiconductor surfaces are 1 to 2 orders of magnitude lower than for clean metal surfaces. Hence, considerably lower electron-stimulated desorption rates can be anticipated for semiconductor surfaces. In fact, we achieved significantly improved long-term cold-cathode performance at even higher collector voltages than applied previously and *without* using an additional magnetic field. Figure 15 shows a life test on a sample operated at 600 V with a close-proximity GaAs anode for a period of over 40 hours. During this period, the total emission current dropped from 95 to 60 µA, representing a decrease in emission efficiency from 1.5% to 1.0%. A similar life test was conducted at even higher emission efficiency and total emission current. Here, during operation at 600 V for 18 hours, the efficiency decreased from 1.9 to 1.45% and the emission current from 190 to 145 µA dc.
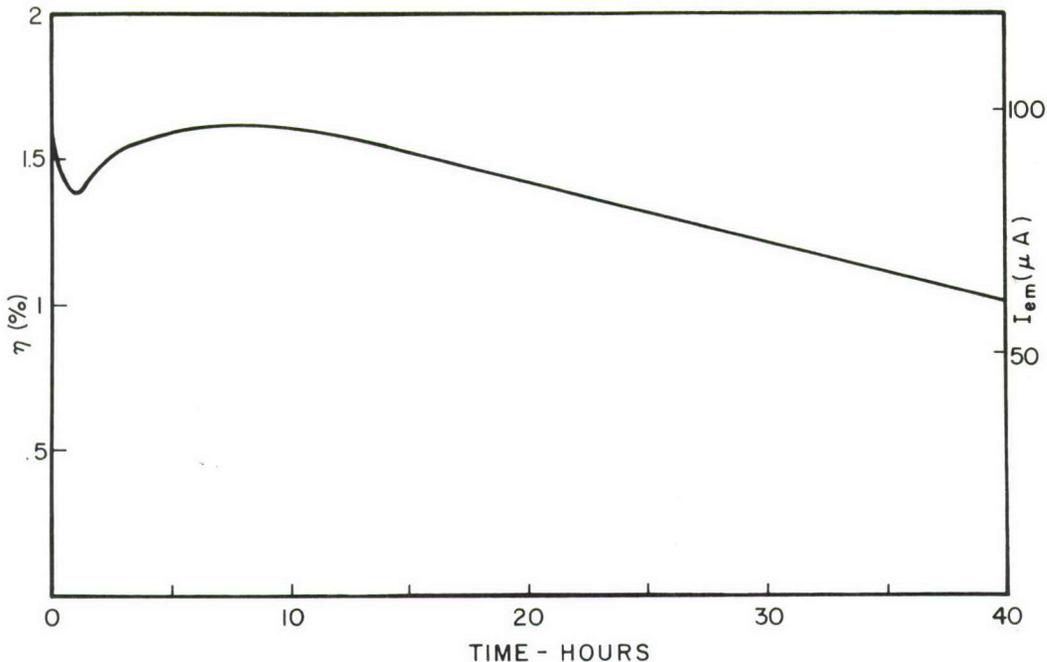
Figure 15. Life test of a cold-cathode operated with a semiconductor anode at a voltage of 600 V. The initial decrease and rise in efficiency is thought to be related to initial electron-stimulated desorption from the anode and a balancing of adsorption and desorption on the cathode surface.

2. Operation in Sealed Tubes

The dc experiments described thus far were conducted in continuously pumped vacuum tubes. With regard to potential applications, we also investigated extended cathode operation in sealed tubes. Based on our previous results with dc operation, we constructed a seal-off tube whose main feature was the incorporation of a GaAs anode to reduce the contaminating effects of electron-stimulated desorption. In this tube, we activated three different optoelectronic samples, but mechanical sample problems prevented the long-term testing of the first two samples. Life-testing of the third sample, however, was successful. The sealed tube was operated at various emission currents (5 to 20 µA dc) and collector voltages (5 to 30 V) for a total duration of 360 hours. The operation was interrupted several times (for periods up to 5 months) to determine if the degradation rates depend on periods of nonoperation. No such dependence could be established. Typically, the emission efficiency showed some recovery upon leaving the cathode inoperative. Continuation of dc operation then resulted in an initially sharp decrease in efficiency to approximately that value at which the previous period of operation had been interrupted. The sample then continued to operate at a considerably smaller degradation rate. Figure 16 shows degradation rates, expressed as the relative change per hour in emission current, as a function of the collector voltage.

20
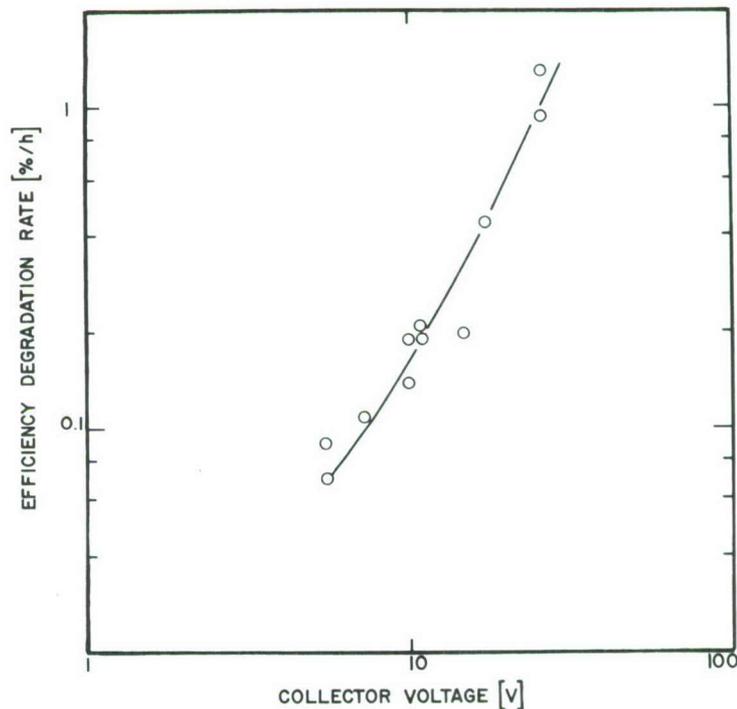
Figure 16. Efficiency degradation rate as a function of the collector
            voltage, measured during dc cathode operation in a sealed
            tube. Each data point represents the relative change in
            emission current over a period of at least 10 hours.

Each point in the curve represents a period of cathode operation of at least
10 hours. Consistent with the mechanism of electron-stimulated desorption[9],
the degradation rate increases with the collector voltage. This is to be ex-
pected, even for GaAs as collector material, although in this case the degrada-
tion rates are orders of magnitude lower than for metal collectors. However,
electron-stimulated desorption normally does not take place below a certain
threshold voltage, i.e., typically below 10 V[9]. The slow degradation which
we found even at collector voltages as low as 5 V, therefore, may be attributable
to the fourth mechanism (4) mentioned before, namely the interaction of the
electron emission with the activated surface.

It is worth mentioning that the degradation rate for sealed tube condi-
tions is, within the limits of accuracy, the same as that measured during ex-
tended operation in a continuously pumped system. For the latter case, the
degradation rate is derived from Fig. 12 to be 0.1 μA/h at 36 μA and 15 V, or
0.3%/h at 15 V. About the same value has been found during cathode operation
in the sealed tube (see Fig. 16).

It thus can be concluded that sealing-off the tube from the pump does not
adversely affect the long-term performance of negative-electron-affinity GaAs
cold-cathodes. Furthermore, due to the recovery in emission efficiency during

21

nonoperation and due to the excellent shelf-life, these cold-cathodes lend
themselves to applications which require intermittent, but instant operation.

C. EFFECTS OF ELECTRON-STIMULATED DESORPTION

    As indicated in Section VI.B.1, the results on long-term cold-cathode
operation suggest that the decrease in efficiency can be attributed to a change
in surface activation, i.e., to a decrease in negative electron affinity. The
surface activation can change either because cesium and/or oxygen are in some
manner removed from the GaAs surface or because of the adsorption of additional
impurities. These may even include additional oxygen, or cesium which would
disturb the desired balance between the concentrations of these two species.

    The experimental evidence so far indicates that the *addition* of impurities
on the GaAs surface desorbed from the *anode* is a key factor in the efficiency
loss of the cathode. This conclusion is based on the observation that a
degraded cold-cathode partly recovers its efficiency by simply allowing it to
stand inoperative at room temperature. A recovery occurs even during dc opera-
tion, if the cathode is operated at an elevated temperature (about 150°C).
The recovery in emission efficiency at high temperature cannot be attributed
to the contribution of thermionic emission, since the emitted current for zero
junction current was more than 4 orders of magnitude lower than the emission-
current increase during cold-cathode operation at elevated temperatures.
Neither can the efficiency increase due to heating be explained by a broadening
of the energy distribution of the electrons to be emitted, since the efficiency
continues to rise even after temperature equilibrium has been reached. The
most probable explanation is that heating of the surface prevents or reduces
the physical adsorption of impurities released from the anode, while the
"balanced" Cs-O layer, which is much more strongly bound to the surface by
chemisorption, is not adversely affected by the 150°C heating.

    The following experiment suggests that oxygen is physically adsorbed and
can cause efficiency degradation. Intentional admission of oxygen into the
vacuum chamber caused the initial efficiency to decrease from 0.18 to 0.003%.
Heating of the cold-cathode structure, however, resulted in a nearly complete
recovery to 0.12% during the next 10 hours, as shown in Fig. 17. Consistent
with oxygen contributing to the efficiency degradation is the fact that oxygen
is one of the main adsorbates on tungsten or tantalum. These materials have
been used here for collectors which were described above to give rise to sub-
stantial electron-stimulated desorption and hence efficiency degradation.

D. ENERGY DISTRIBUTION OF ELECTRONS EMITTED FROM A NEGATIVE-ELECTRON-AFFINITY
    GaAs-(AlGa)As COLD-CATHODE

    Since semiconductor cold-cathodes operate at room temperature, they are
expected to have a narrower energy distribution of the emitted electrons than
conventional thermionic cathodes operating at about 1000 K. This would repre-
sent a major advantage in all beam-focusing and imaging applications and would
result also in reduced beam-discharge lag in camera tubes, for instance. A
second advantage implied by cold-cathode emission is lower noise which may
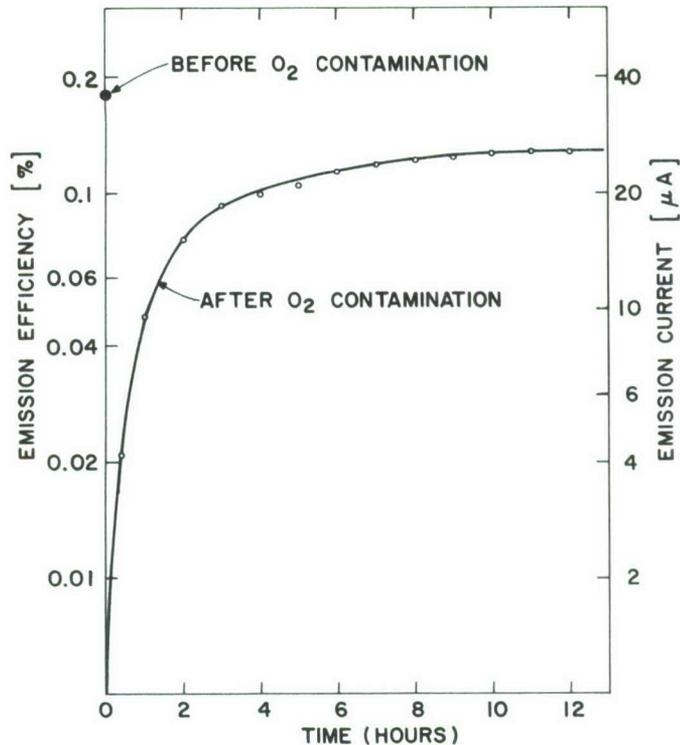
Figure 17.   DC operation of a cold-cathode at 150°C after admission
             of oxygen, showing an efficiency recovery.

lead to higher signal sensitivity of devices incorporating cold-cathodes rather
than thermionic cathodes.   Finally, devices incorporating cold-cathodes require
no heat shielding, which greatly simplifies the construction of infrared-sensing
devices.

    We have concentrated our efforts on experimentally verifying the narrow
energy distribution of a negative electron affinity cold-cathode which - to
our knowledge - has not been measured before.   In order to do this measure-
ment, we have designed and constructed a tube to apply a retarding field tech-
nique.   The principle of this technique is shown in Fig. 18, in the upper
portion in terms of the energy band diagram of the electrodes involved, and in
the lower portion schematically in terms of the actual electrodes in the tube.
The cathode is surrounded by a hemispherically shaped grid electrode, beyond
which a collector electrode is located.   The retarding voltage on the grid is
varied in such a way that only electrons above a certain kinetic energy can
reach the grid and subsequently be collected by the collector.   The collected
current as a function of the retarding voltage contains the information on
the energy distribution of the emitted electrons.   By using lock-in techniques
and thus differentiating the collected current with respect to the retarding
voltage, the energy distribution can be readily displayed.

    The construction of the retarding field electrode was led by two considera-
tions: (1) The electrode was shaped into a hemispherical shell in order to
preserve the angular distribution of the electrons as they are emitted.   (2) The
electrode transmits electrons only through a small hole directly opposite the
emitting surface.   Thus, the electrons are selected only from a small solid
angle in which field distortions can be neglected.

23
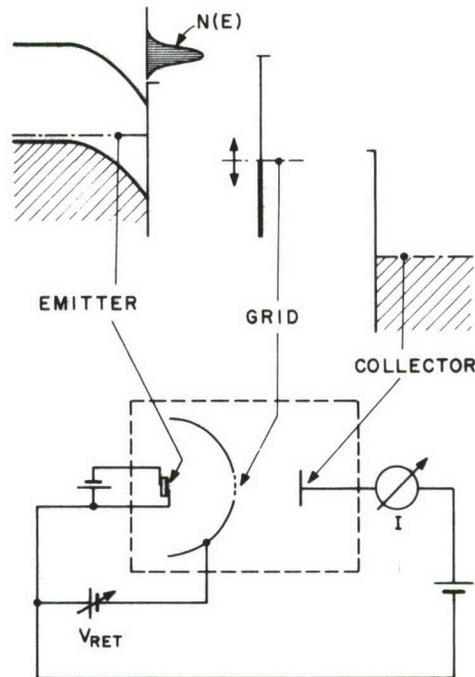
Figure 18. Retarding field technique for electron energy
            distribution measurement.

    In our experiments, we used a GaAs-(AlGa)As heterojunction structure
operating with direct electron injection (see Fig. 5). We used this structure
because it allowed us to obtain a smaller emitting area than with the opto-
electronic structure. A small emitting area, approaching as closely as possible
a true point source, is essential to obtain reliable energy distribution data.
The experimental results equally should hold for an optoelectronic emitter,
since the supply of electrons to be emitted consists, in both cases, of ther-
malized electrons in the Ge-doped p-type GaAs top layer of the structure.

    The energy distribution of a sample exhibiting a total emission efficiency
of 2% is shown in Fig. 19. Also shown in the same energy scale is the spatial
dependence of the lower conduction band edge in the surface region. The con-
clusion to be drawn from this figure is that essentially monoenergetic elec-
trons reaching the bent band region become subject to a spread in their energy
upon emission from the surface. The half-width of the measured energy dis-
tribution (solid line) was found to be 160 meV, which equals about 6 kT at
room temperature. This half-width is distinctly smaller than that of a con-
ventional thermionic cathode, which at 1000 K would give rise to a half-width
of 220 meV (see Fig. 20).

    Thus, we obtained the first experimental proof that the energy distribu-
tion of a GaAs cold-cathode based on negative electron affinity is, indeed,
narrower than in the case of conventional hot-cathodes.

    However, the measured width of 6 kT requires some explanation, since it
might seem larger than expected. Based on a model by Bartelink et al.[11],
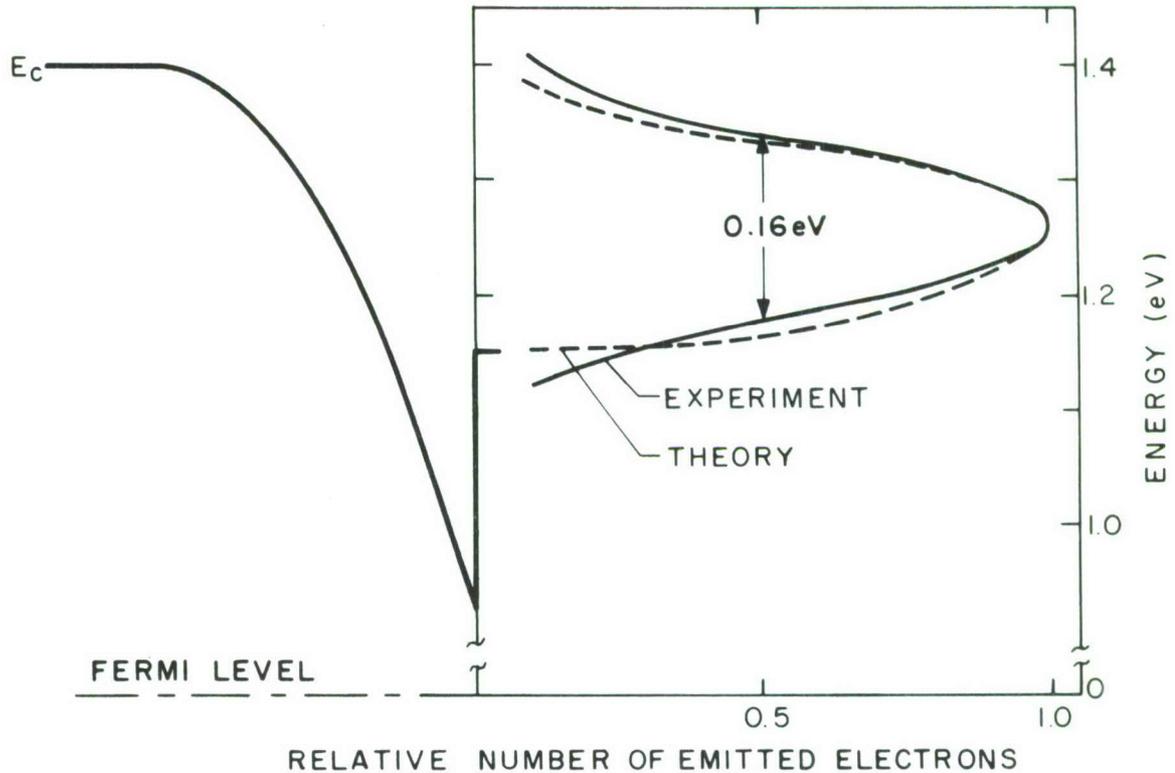
Figure 19.   Energy distribution of electrons emitted from a GaAs cold-cathode;
             also shown in the same energy scale is the spatial dependence of
             the conduction band edge adjacent to the emitting surface.
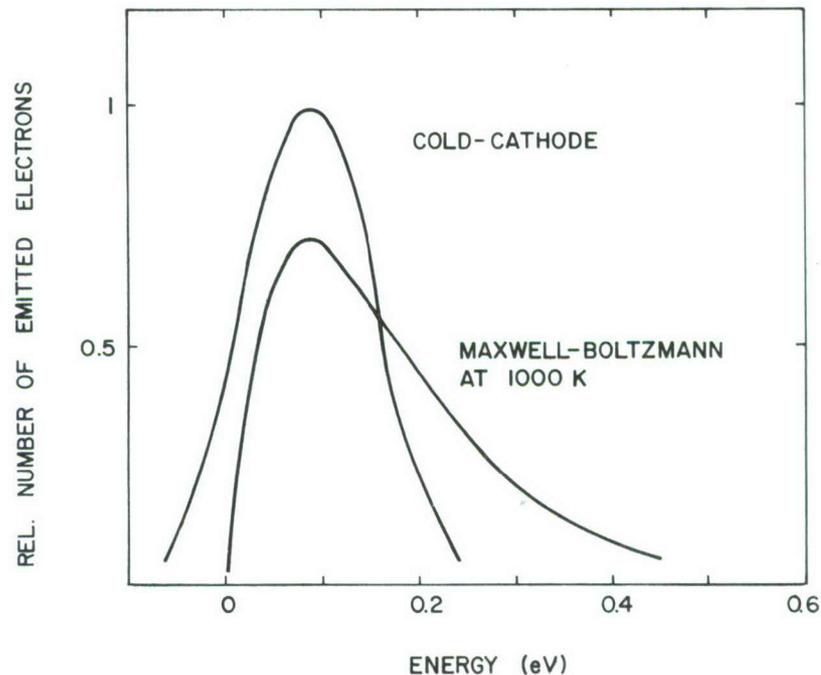
Figure 20.   Energy distribution of electrons emitted from a GaAs cold-cathode
             and from a conventional thermionic cathode (Maxwell-Boltzmann
             distribution).   The curves were matched at their maxima and
             normalized to equal total emission.

we have, therefore, calculated the energy distribution of the electrons being emitted from the semiconductor. Here one must consider that the electrons reaching the surface space-charge region are accelerated by the internal electric field in this region, but at the same time become subject to energy losses to optical phonons. These interactions are characterized by a mean free electron path ℓ_p between two collisions with optical phonons and by an energy loss ΔE_p per collision. Besides these collision parameters, the total energy loss E_p of each electron depends on the number of collisions the electron suffers on its way to the surface. This number, in turn, is a function of the thickness d of the space charge region which is given by the doping concentration of the semiconductor material. The effect of doping on the energy distribution of electrons reaching the surface is illustrated in Fig. 21. The curves shown here are calculated from a solution of the Boltzmann transport equation which
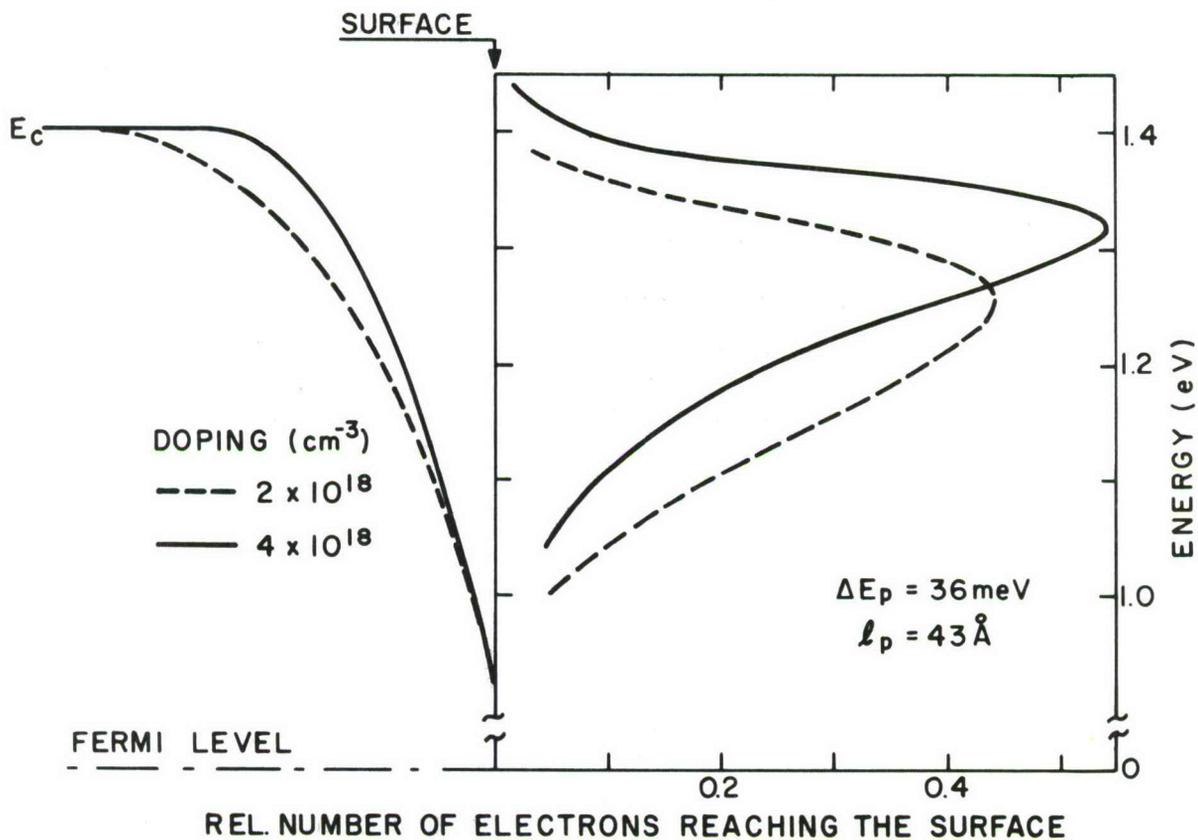
Figure 21. Energy distribution of electrons reaching the surface, but prior to being emitted.

has been given by Bartelink et al.[11] in general form and has been modified by us to the conditions of our present problem. If we neglect ionization losses of the electrons, this modified solution takes the form:

$$N(E_p) = \text{const.} \; [(V/E_p)^2 - (V/E_p)] \; \exp \; [3/4(d/\ell_p)^2 (\Delta E_p/E_p)] \qquad (7)$$

26

assuming

$$V - E_p \gg (F\ell_p)^2/6\Delta E_p \text{ and } F = V/d \qquad (8)$$

where, in addition to the quantities mentioned above, V is the amount of band-bending and F is the electric field in the bent-band region.

By multiplying Eq. (7) with an energy-dependent surface escape probability P_W, one obtains the energy distribution of electrons being emitted from the surface, as shown by the dashed curve in Fig. 19. This curve was obtained by assuming a work function of W = 1.15 eV for the cesiated GaAs surface and a simple step function potential barrier at the surface. For this barrier, P_W is given by

$$P_W = \frac{4\sqrt{V-E_p}\sqrt{E_g-W-E_p}}{\left(\sqrt{V-E_p} + \sqrt{E_g-W-E_p}\right)^2} \qquad (9)$$

where E_g is the bandgap of the semiconductor material and W the work function of the cesiated surface (note that $E_g > W$ for negative electron affinity).

The comparison between the experimental and theoretical energy distribution indicates that the measured half-width of about 6 kT is consistent with theoretical expectations. The remaining discrepancies between the two curves lie well within the limits of the experimental energy resolution.

Finally, in comparing the energy distributions emitted from a cold-cathode and a thermionic cathode we note, in addition to different half-widths, a significant difference in the shape of the distribution. This difference is illustrated in Fig. 20 by showing our measured distribution and a Maxwell-Boltzmann distribution emitted from a thermionic cathode at 1000 K[12]. While for thermionic cathodes there is a distinct exponential high energy tail, the cold-cathode distribution falls off rather sharply toward high electron energies, which is a considerable advantage in all beam-focusing and beam-landing considerations.

VII. INCORPORATION OF GaAs-(AlGa)As COLD-CATHODES INTO EBIT STRUCTURES

A. PRINCIPLE OF THE ELECTRON-BEAM-INJECTED TRANSISTOR (EBIT) AMPLIFIER

The underlying principle of the EBIT amplifier is the current multiplication in a reverse-biased semiconductor element, such as a p-n junction or a Schottky-barrier diode, bombarded by a high-velocity electron beam (Fig. 22). If the velocity of the electrons is sufficiently high (5 to 10 keV), the beam will penetrate the semiconductor material and its energy will be dissipated in creating electron-hole pairs. For example, in silicon, the energy required for creation of a pair is 3.6 eV. If penetration losses are neglected, a primary electron having an energy of 10 keV would create approximately 2800 ($= 10^4/3.6$) electron hole pairs. Under proper reverse bias, the current gain would be also 2800. In practice, the penetration losses caused by surface metallization required for dc and rf contacts, recombination of electrons and holes, and other effects reduce the current gain. In silicon, the current gain in a practical p-n junction is approximately 2000 for a 10-keV electron beam. The high current multiplication in the output together with the low-power, wide-band modulation capability of the electron applications, such as linear phase-stable amplifiers having a power capability of 20 to 30 W cw at S-band, and pulsed amplifiers of over 100 W at L-band. The EBIT amplifier promises discrete advantages as compared with regular travelling-wave tubes on the one hand and purely solid-state amplifiers on the other.

This program was designed to assess the feasibility of using an optoelectronic cold-cathode as source of the electron beam instead of a conventional thermionic electron emitter. In particular, it will be determined, whether the cathode activation affects the current gain of the semiconductor EBIT target.
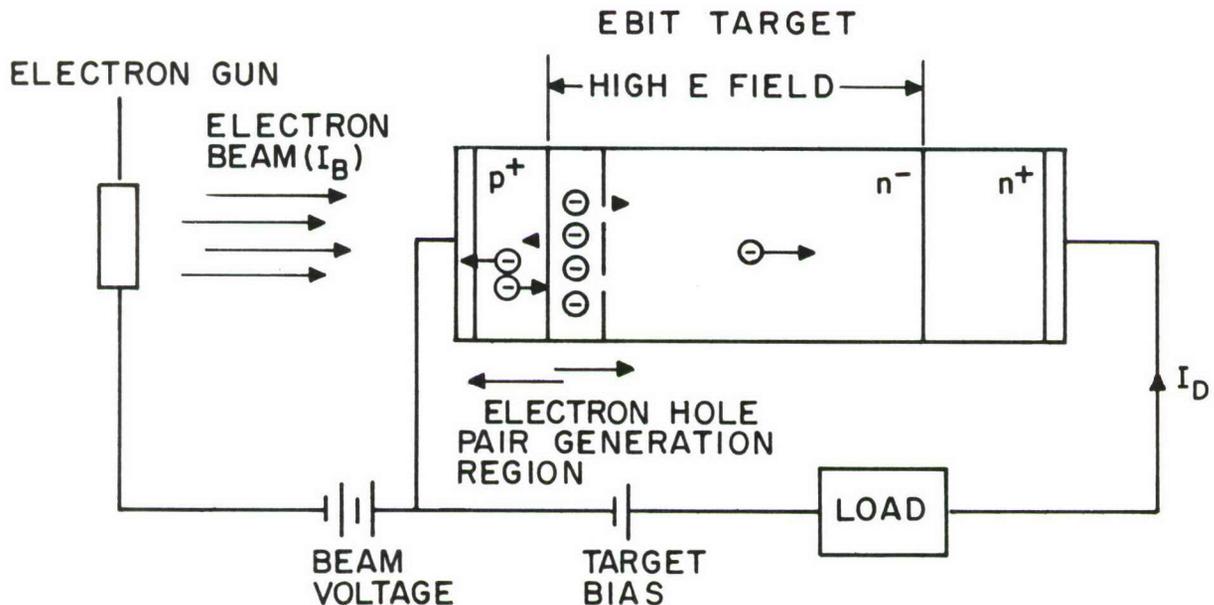
Figure 22. Principle of EBIT operation.

B. DESCRIPTION OF EBIT TARGET AND TEST VEHICLE

The EBIT target used in the test vehicles was a silicon-dioxide and poly-silicon passivated silicon planar p-n junction. A cross-sectional view of such a junction is shown in Fig. 23. The purpose of the polysilicon layer (resistivity $\sim 3 \times 10^6$ ohm-cm) was to provide the voltage divider (or distributed gate) action for spreading the electric field lines away from the edges of the junction and thereby achieve a high voltage breakdown. The silicon dioxide and the aluminum film around the periphery of the junction are used for protection from stray high-voltage electrons.
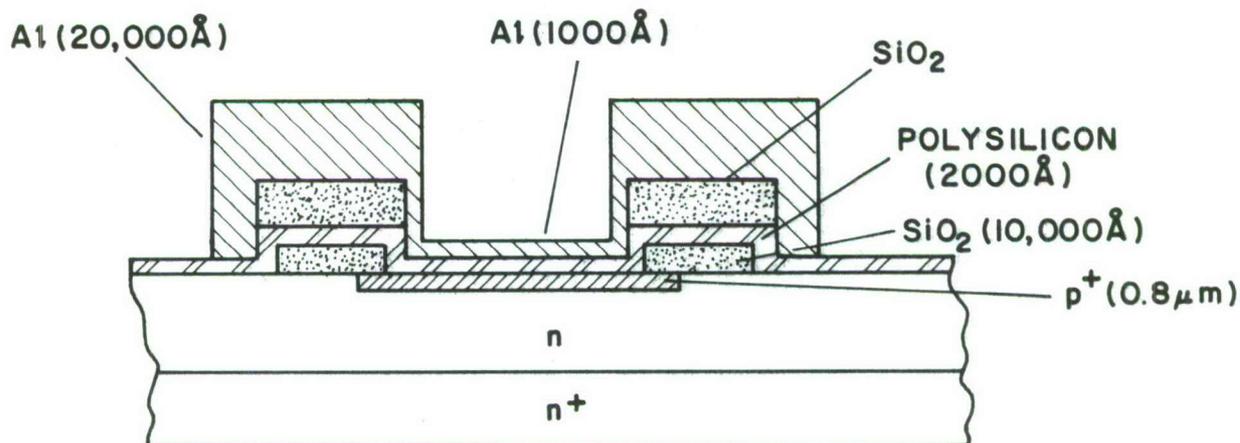
Figure 23. Cross section of the EBIT target, consisting of a planar silicon dioxide and polysilicon passivated silicon p-n junction.

Figure 24 shows the top view of the junction mounted on a threaded stud. The external dimensions of the chip were 0.032 in. x 0.113 in., and the active area was 0.020 in. x 0.095 in. The chip was mounted on a beryllium-oxide pad that included metallized patterns for bonding the target and contact wires. These features are seen clearly in Fig. 24.

Figure 25 shows a simplified cross-sectional view of the elements mounted in the test vehicle and the circuits used for measurement of current gain and operation of the optoelectronic cathode. Figure 26 is the photograph of the complete tube. The oxygen leak, used for cathode activation, can be seen clearly in the lower center of the photograph. The upper portion shows the bellows for holding and moving the anode aperture electrode. This electrode was displaced during activation to permit direct exposure of the cathode to cesium and oxygen. The diameters of the apertures in these electrodes were 0.010 in. and 0.030 in., and the materials were tantalum and gallium-arsenide, for the first and second tubes, respectively.
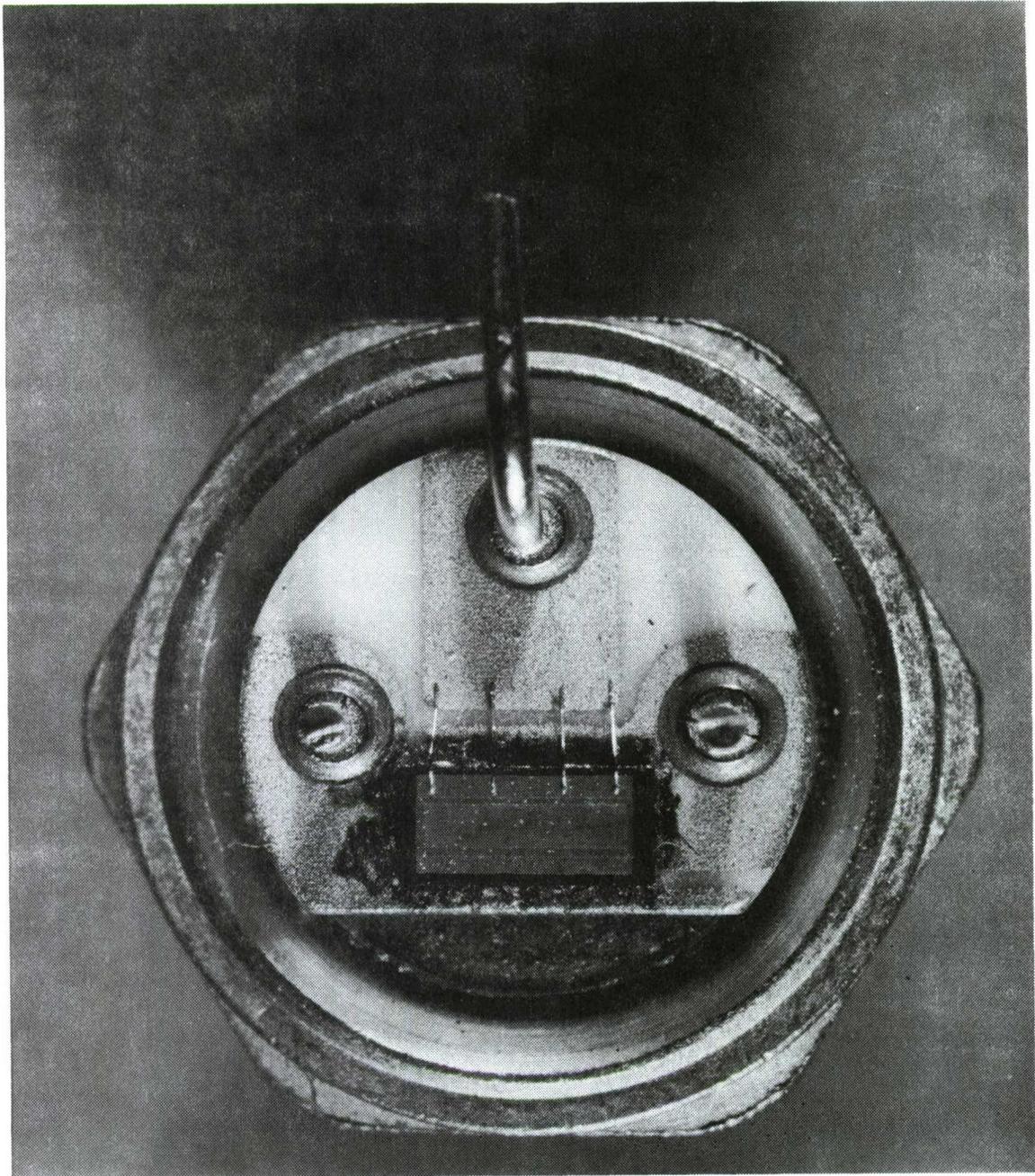
Figure 24. Top view of the passivated silicon p-n junction
bonded to a threaded stud.
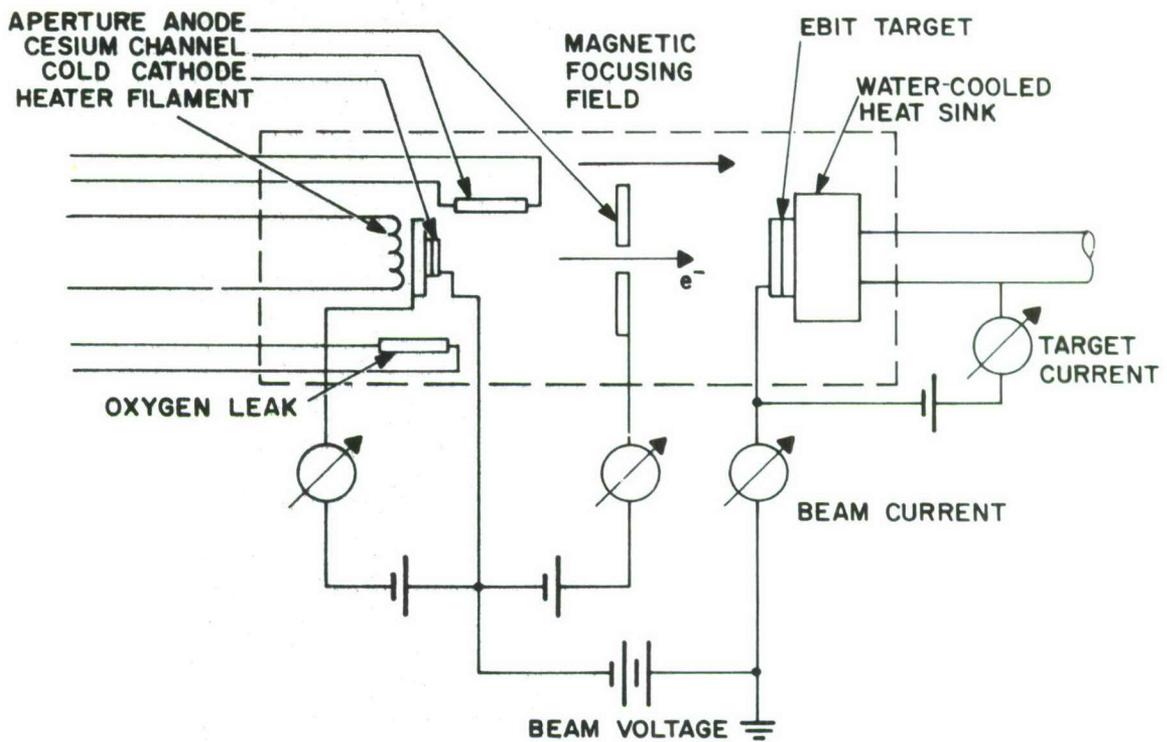
Figure 25. Test circuit for current gain measurement.
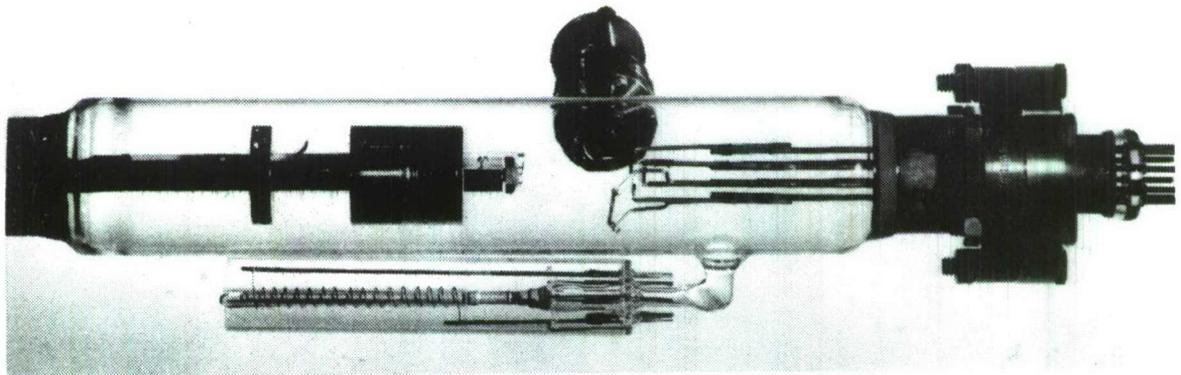
Figure 26. EBIT test tube, incorporating an optoelectronic cold-cathode. The cathode is mounted on the right feedthrough assembly; the aperture anode is held by a bellows mounted on a mini-flange, which can be seen in the center of the photograph; also visible in this area are the cesium channel and the attached silver oxygen leak. The left part of the tube contains the EBIT target, mounted on a heavy water-cooled heat sink.

C. STUDY OF REVERSE CHARACTERISTICS OF THE EBIT TARGET DURING ACTIVATION OF THE COLD-CATHODE

One of the major objectives of the target-evaluation phase of the program was the study of the effects of cesium-oxygen activations of the cathode surface on the reverse current-voltage characteristics of the target. For this purpose, a record of I-V traces was maintained throughout the processing cycle. These characteristics will now be described in some detail.

Figure 27(a) shows the reverse current-voltage trace of the target before processing. The theoretical bulk breakdown for the target is 264 V. Inspection of Fig. 27(a) indicates that the target did not break down up to the voltage of 200 V, or 76% of the theoretical value. The trace was not extended above 200 V to prevent catastrophic failure of the target.

Figure 27(b) shows the trace recorded after a 200°C, 20-hour, vacuum bake-out. Voltage breakdown was not observed up to the maximum tested value of 180 V; i.e., there was no serious degradation after bake-out. However, the reverse leakage current doubled.* Prior to the surface activations, cesium was released into the tube at about 200°C for "cleaning" purposes. Subsequently, the leakage current reached 1 mA at 155 V, as shown in Fig. 28(a). This was the highest leakage recorded throughout the whole processing cycle. After a 235°C, 15-hour vacuum bake-out and conventional cesium-oxygen activations at room temperature (see Section V) a leakage of 1 mA was obtained at a voltage of 185 V, as shown in Fig. 28(b). Comparison of this trace with that shown in Fig. 27(b) indicates that the reverse I-V characteristic after cathode processing is essentially identical to that obtained before processing.

The I-V traces recorded during processing for the second tube were comparable to those described above for the first target.

D. CURRENT GAIN CHARACTERISTICS

The *solid* curves in Fig. 29 show the current gain as a function of beam voltage for two EBIT tubes employing optoelectronic GaAs-(AlGa)As cathodes. The dashed curve is the typical characteristic obtained for the silicon dioxide and polysilicon passivated silicon p-n junction by use of thoria and oxide cathodes. The first tube provided slightly higher gain and the second tube slightly lower gain than the typical characteristic.

Thus, we have obtained the relatively high current gain of 1180 at a beam voltage of 9 kV, as compared with a gain of 930 at 9 kV for the second tube. However, both gain characteristics are sufficiently close to the typical target performance to conclude that the cesium-oxygen activations of the optoelectronic cathode did not cause the electrical characteristics of the target to deteriorate.

---

*This increase of leakage after bake-out is typical for silicon-dioxide passivated devices and is caused by release of positive charges from the dioxide. Aluminum oxide and polycrystalline passivations are now under development to provide better target stability.
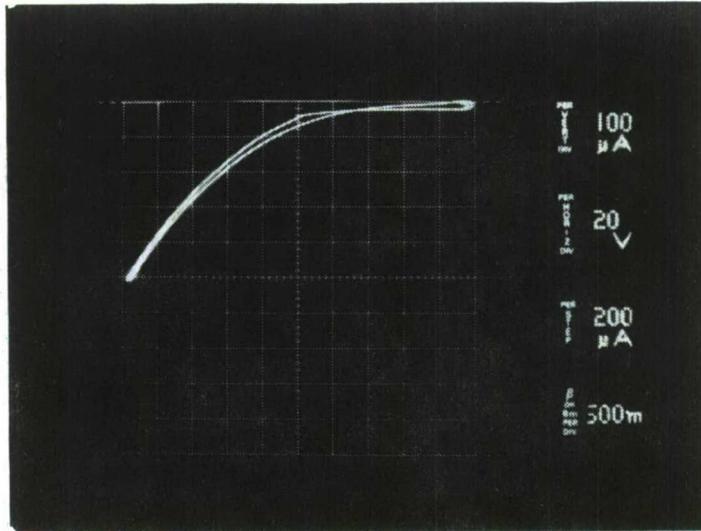
(a)
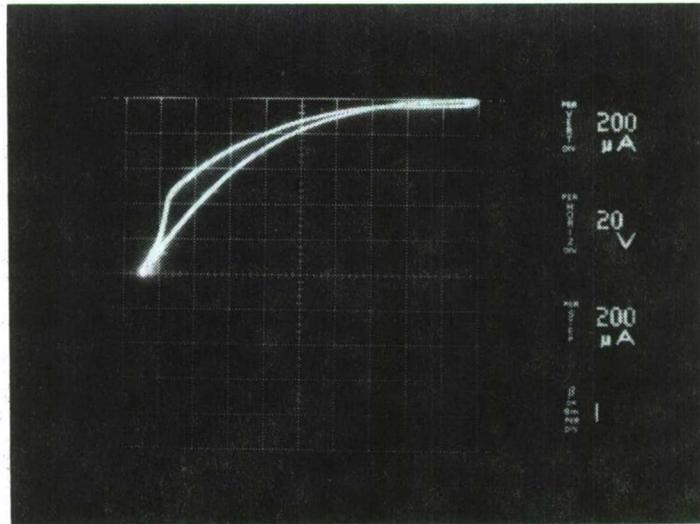
(b)

Figure 27.   Reverse current-voltage characteristics of the EBIT target
            (a) before processing and
            (b) after a 200°C, 10-hour vacuum bake-out.

33
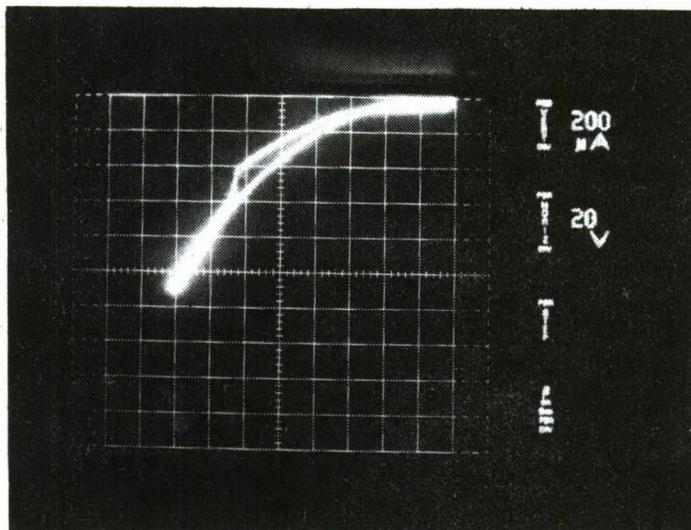
(a)
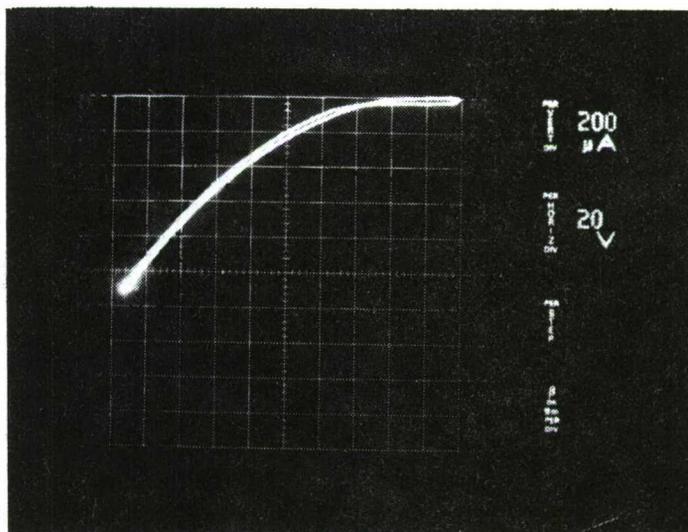
(b)

Figure 28. Reverse current-voltage characteristics of the EBIT target
(a) after heavy cesium exposure and
(b) after completion of cathode processing.
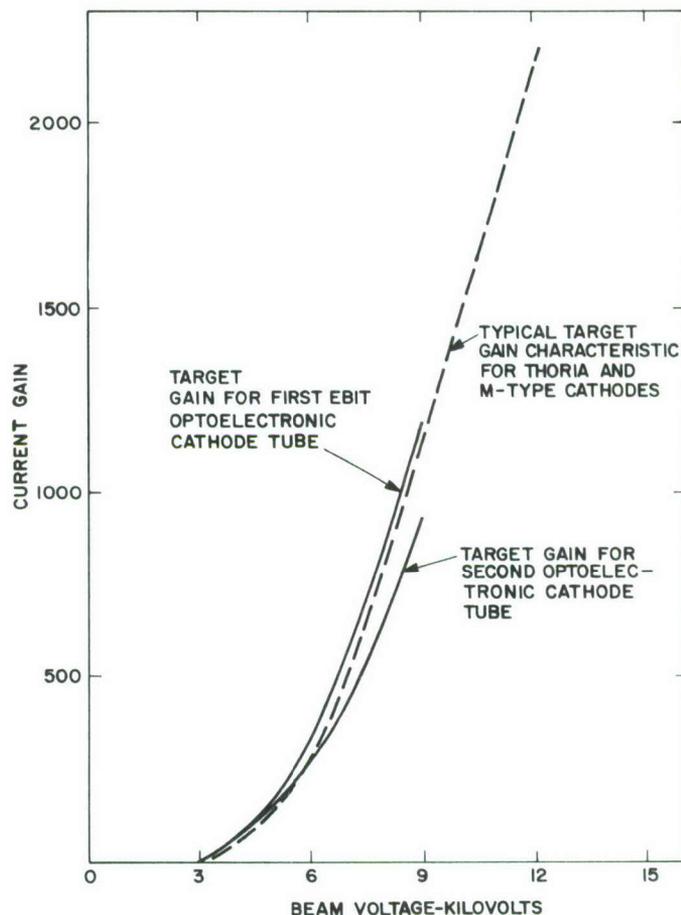
Figure 29.   Current gain as a function of the beam voltage for two
EBIT tubes employing optoelectronic cold-cathodes.

The critical voltage for both targets employing the optoelectronic cathode
was approximately 3 kV (Fig. 29), a value identical to that measured for other
types of cathodes. This feature confirms again that the cesium-oxygen activa-
tions did not create lossy layers on the surface of the target that might
reduce the electron energy.

The gain curves shown in Fig. 29 were measured at beam currents ranging
from 0.5 to 3.0 µA and target voltages up to 9 kV at junction currents from
20 to 35 mA and junction voltages between 1.8 and 2.4 V. It must be noted,
however, that the cold-cathode emission during standard test procedures at
collector voltages of 300 V was much higher, namely, up to 30 µA dc at 20-mA
junction current, i.e., 0.15%. No attempts were made to further improve the
emission efficiency since the obtained emission currents were fully sufficient
to conduct the EBIT current gain experiment.

The anode electrode was displaced during measurements of the current gain,
and the beam current was drawn directly from the cold-cathode by the acceler-
ating beam voltage. A magnetic focusing field, produced by Helmholtz coils,

was used to bring the beam into focus at the target. The relatively simple mechanical design of the cathode, anode, and target assemblies did not permit simultaneous alignment of the beam through all these elements in presence of the magnetic focusing field. Although excellent ($\sim$ 100%) beam transmission was achieved through the anode aperture in the absence of focusing, application of the magnetic field deflected the beam to the solid portion of the anode, and the resulting release of impurities caused a reduction in the cathode emission efficiency (see Section VI. B). In the second tube, which employed the larger 0.03-in.-diameter aperture in GaAs, this problem was less severe than in the first tube. However, since the alignment of the critical element was not ideal, the gain measured in presence of the anode electrode was only one-half that obtained when this electrode was displaced. The above difficulties indicate that additional development is necessary for incorporating the optoelectronic cold-cathode into a useful electron gun structure, which includes one of the necessary features discussed in Section VI. B. to avoid contamination of the cathode surface.

E. TENTATIVE EBIT AMPLIFIER DESIGNS

In this section we will consider briefly the ability of the optoelectronic cold-cathode to meet the requirements for typical EBIT amplifier designs. The type of amplifier to be evaluated is a linear, class-A device employing cylindrical helix and electron beam in the input circuit, similar to those used in conventional travelling-wave tubes (type-0), and a single target mounted in a coaxial output section.

Table II lists the operating parameters for a 20-W cw S-band tube.

TABLE II

Tentative Design and Operating Parameters for
a 20-W CW EBIT S-Band Amplifier

Power output	20 W cw
Frequency range	2-4 GHz
RF power gain	35 dB
Efficiency	27.4%
Beam voltage	12,000 V
Beam current	1.25 mA
Effective beam diameter	0.035 in.
Beam current density	0.2 A/cm^2
Target current gain	2000
DC output current	2.5 A
Active target diameter	0.035 in.
Length of input helix	3 in.
Overall tube length	5.5 in.
Maximum dimensions	1 in. x 1 in. x 5.5 in.
Weight	6 oz max.

The important parameters in considering the applicability of the optoelectronic cold-cathode for the above design (Table II) are the beam diameter (0.035 in.) and the beam current density (0.2 A/cm^2). Both quantities are achievable with these cathodes. The tests described previously indicate that the beam diameter produced by the optoelectronic cathode was in the range from 0.020 to 0.225 in. The maximum cw current density demonstrated under laboratory conditions is about 0.4 A/cm^2, a value approximately twice that required for the tentative design listed in Table II. Therefore, operation of this design in conjunction with the optoelectronic cold-cathode is, in principle, feasible.

Another tentative design, shown in Table III, is directed at a 250-W, pulsed, L-band amplifier. Of particular interest in this design is the relatively short overall length (4 in.) of the amplifier, several times smaller than the size of comparable state-of-the-art travelling-wave amplifiers. The effective beam diameter of 0.068 in. and the peak beam current density of 0.140 A/cm^2 can be provided by the optoelectronic cold-cathode.

Other advantages of the optoelectronic cold-cathode over thermionic cathodes are essentially instantaneous "warm-up time" and the ability to provide pulsed operation by pulsing the junction current rather than the voltage on a grid. Absence of the grid results in improvement of beam focusing and elimination of secondary emission and power-dissipation problems.

TABLE III

Tentative Design and Operating Parameters
for a 250-W Pulsed L-Band Amplifier

Peak power output	250 W
Pulse length	5 μs
Duty cycle	5%
Frequency range	1-2 GHz
RF power gain	35 dB
Efficiency	35%
Beam voltage	12,000
Beam current	3.23 mA
Target current gain	2000
Effective beam diameter	0.068 in.
Beam current density	0.14 A/cm^2
DC output current	6.45 A
Active target diameter	0.068 in.
Length of input helix	1 in.
Overall tube length	4 in.
Weight	6 oz

Furthermore, the narrower energy spread of electrons emitted from a semiconductor cold-cathode (160 meV as compared with 230 meV for a thermionic

cathode, see Fig. 20) is expected to lead to a smaller noise figure. In travelling-wave tubes, for example, the noise figure is given by:

$$NF = 1 + \frac{T_c}{T_o} \frac{(S-\pi)}{\pi_o} \tag{10}$$

where T_c is the cathode temperature, T_o is room temperature, and the functions S, π, and π_o depend on the circuit and beam parameters. The noise figure is determined predominantly by the effective cathode temperature. A state-of-the-art S-band travelling-wave tube has a typical noise figure of 5 dB. This indicates that for the thermionic cathode the second term in Eq. (10) is numerically equal to approximately 2. For the cold-cathode this term becomes equal to $2 \times \frac{0.160}{0.230} \approx 1.4$; the noise figure is then 4 dB. Thus, the cold-cathode reduces the noise figure by 1 dB.

Finally, it is worth noting that the power required to generate a certain emission current is considerably lower for the optoelectronic cathode than it is for an oxide cathode. Thus, to obtain a beam current of 1.25 mA, for instance (see Table II), a cold-cathode structure emitting at an efficiency of 2.5% requires a power input of about 150 mW (50 mA at 3 V), whereas a heater power of 1.6 W (0.25 A at 6.3 V) is needed for an oxide cathode.

VIII. CONCLUSIONS

It has been shown for the first time that semiconductor cold-cathodes based on negative electron-effinity surfaces in III-V compounds are capable of operation at efficiencies and emission-current densities of practical interest.

A greatly improved cold-cathode emitter structure has been developed based on the use of liquid-phase epitaxy and GaAs-(AlGa)As heterojunctions. The key to the successful development of this device was the ability to obtain GaAs with electron-diffusion lengths as high as about 5 to 7 μm, and a technique for the confinement of the carrier flow to the desired emitting area.

Efficiencies as high as 4.2% have been achieved under pulsed operation (up to 10% duty cycle) which represents improvement by a factor of about 35 since the start of this program. Pulsed emission-current densities as high as 7 A/cm^2 have so far been observed. These values should not be considered as the limiting ones for this type of device, since cathode heat sinking is a dominating factor in limiting the maximum current density.

Efficient dc operation has been repeatedly obtained. The highest efficiency value was 1.9%, with reproducible values above 1%. The emission currents drawn have been as high as 190 μA, and current densities have reached 0.4 A/cm^2.

A key property of the semiconductor cold-cathode, namely the energy distribution of the emitted electrons, has been measured for the first time. The half-width of the energy distribution of electrons, emitted from a GaAs-(AlGa)As structure, was found to be 160 meV which is distinctly narrower than that for a conventional thermionic cathode. The measured half-width is in fair agreement with calculations that take into account energy losses suffered by the electrons in the space charge region below the surface.

Extensive studies on dc operation and cathode life have been conducted under continuously pumped vacuum conditions as well as in sealed tubes. No significant difference in cathode performance has been observed for these two ambient conditions. Shelf-life of cathode efficiency in sealed tubes has been measured to be essentially constant for a period of up to 5 months. In one experiment, for example, the emission efficiency changed only from 2.0 to 1.9% during a period of 2 months, after which the tube had to be delivered to the Contracting Agency.

During dc operation, the emission efficiency decreases with time. Operation with a GaAs anode at 600 V for 18 hours, for instance, caused the efficiency to decrease from 1.9 to 1.45% and the emission current from 190 to 145 μA dc. We have determined some of the reasons for emission efficiency degradation during dc operation. A major source for rapid degradation is electron-stimulated desorption from the collector electrode. In this process, the collected electrons give rise to desorption of impurities from the collector which then are, in part, readsorbed on the emitting surface and are thus responsible for a deterioration of the surface activation. Cathode life, therefore, can be greatly extended by using either of the following three methods.

1. Operation at sufficiently low collector voltages ($\lesssim 15$ V), at which essentially no electron-stimulated desorption occurs.
2. Application of a magnetic field which separates the paths of electrons and ions and eliminates possible sputtering of the emitting surface.
3. Use of GaAs, instead of tungsten, as a clean collector material.

All these methods have been found to lower the degradation rates by orders of magnitude as compared with cathode operation in a simple vacuum diode design. Thus, the smallest relative decreases of the dc emission current, obtained over periods of more than 20 hours in a sealed tube with a GaAs collector, ranged from 0.07 to 1%/h at collector voltages between 5 and 30 V. With these degradation rates, this particular sealed tube was operated for several periods of 20 to 50 hours or a total of 360 hours. The degradation rates did not change even after shelf-storage for up to 5 months. Moreover, the emission efficiency remained practically constant during these storage periods.

The residual degradation rate found at collector voltages as low as 5 V suggests that there is still a cause for slow emission degradation which has not been accounted for thus far. The excellent shelf-life of the cold-cathodes, however, offers the possibility to use such cathodes in applications which require intermittent but instant operation.

Finally, optoelectronic cold-cathodes instead of conventional thermionic cathodes have been incorporated into electron-beam-injected transistor (EBIT) tubes. The use of cold-cathodes in these tubes will provide for essentially instantaneous "warm-up," pulsed operation by pulsing the cathode junction current rather than a grid voltage, lower noise, and lower power requirements. As the specific purpose of this part of the program, it was shown that the activation procedures did not adversely affect the performance of the EBIT targets. Their reverse current-voltage characteristics did not degrade, and the current gains (≈ 1200 at 9 kV) and threshold beam voltages measured with electron beams from optoelectronic cathodes were essentially identical to those obtained from conventional oxide and thoria cathodes.

Additional development - directed at improvement of cathode life, gun design and beam control between the cathode and target - is necessary to operate EBIT tubes over extended periods of time and at higher power levels. Tentative cw and pulsed amplifier designs indicate that the beam diameters and current densities required for these designs are in the ranges which have been already demonstrated for these cathodes. Approximate calculations have shown that the lower effective temperature of the cold-cathode would reduce the noise figure of a state-of-the-art S-band travelling-wave tube from 5 to 4 dB.

In summary, compared with conventional thermionic cathodes, the semiconductor cold-cathodes developed in this program offer the following advantages:

1. Instantaneous operation, since no cathode heating is required.
2. Simplicity in pulsed operation by pulsing the junction current without the need for an additional modulating grid.
3. Lower noise due to a narrower energy distribution of the emitted electrons.
4. Lower power requirements to provide electron emission.

However, the problem of cathode life requires further investigations. Although there is practically no efficiency degradation during periods of non-operation, relatively slow degradation persists, even under optimum conditions in exploratory test tubes. While the mechanism for this slow degradation needs to be explored by basic surface research on the emitting surface, the cathode life in practical tubes, such as the EBIT tube, is expected to be significantly improved by more elaborate tube engineering involving improved electron beam optics and possibly ion trapping.

APPENDICES

APPENDIX I

SURFACE ESCAPE STUDIES

Our previous photoemission studies on liquid phase grown GaAs:Ge[13] indicated that the electron escape probabilities for our emitting surfaces are about a factor of 2 lower than the highest values reported for GaAs also grown by liquid phase epitaxy[14]. Since the cold-cathode emission efficiency is directly proportional to the surface escape probability, and since we found the process of surface activation to depend on the surface treatment prior to mounting the sample into the vacuum chamber, we performed a series of photoemission experiments to investigate various surface preparations which might lead to an improved surface escape probability. Besides the usual etching in a mixture of H_2SO_4, and H_2O_2, and H_2O, we tried a subsequent etch in H_2O_2, and also a heating in hydrogen prior to mounting the sample into the vacuum system. All these treatments led to about the same photosensitivities. We also tried *in situ* heating of the sample in hydrogen just prior to the activation process. But thereafter the photosensitivity was lower by a factor of two. We did find, however, that the original photosensitivity, 800 μA/lm, could be restored after ion bombardment with cesium or oxygen, followed by a 15-minute annealing step. At the same time, the photosensitivity after this procedure was considerably more stable than before.

Furthermore, we studied <111B> GaAs surfaces which reportedly[14] exhibit higher escape probabilities than the <100> surfaces used thus far. While our previous results on <100> surfaces could be reproduced with <111B> surfaces, an improvement with these surfaces has not yet been found.

In connection with these surface studies, we also checked whether the usual heat cleaning of the surface in vacuum might produce any facetting. Heated and unheated <100> surfaces were tested by scanning electron microscopy, but no obvious signs of facetting could be detected. The heated sample, however, did show signs of decomposition, as indicated by small droplets of possibly Ga, about 1/2 μm in diameter. The results of these studies are shown in Fig. 30. It is worth mentioning that after heating GaAs to closely below its decomposition temperature (∿ 630°C), the surface exhibits a slightly dull appearance which can be correlated with the formation of Ga droplets. However, the photosensitivities of such surfaces are not adversely affected.

43
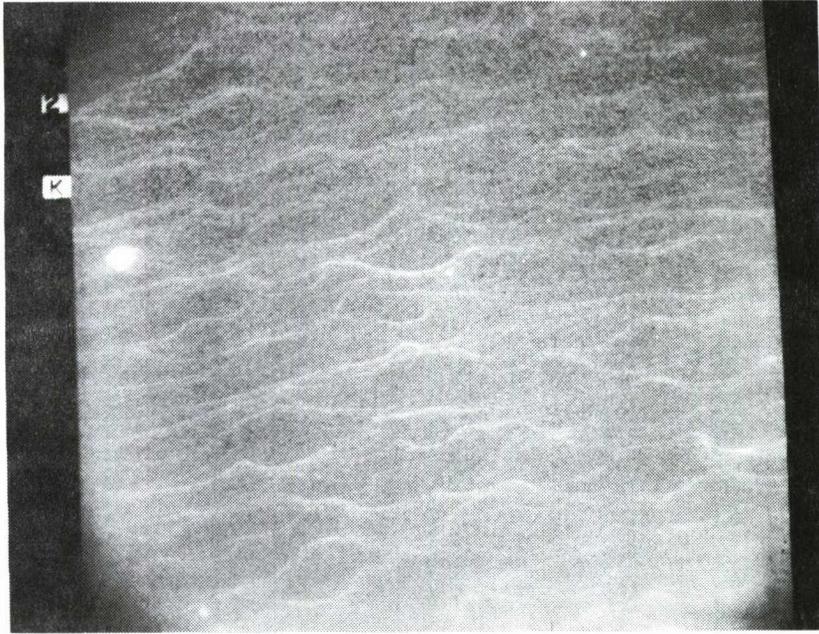
(a)
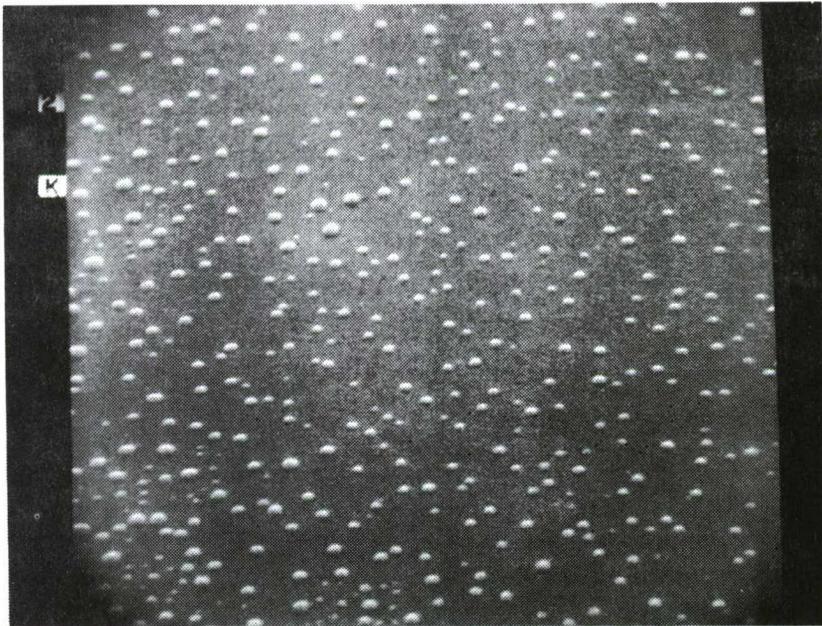
(b)

Figure 30.   Scanning electron micrographs of a <100> GaAs surface
             (a) before and (b) after heating in vacuum to about
             600°C.

APPENDIX II

DIFFUSION LENGTH MEASUREMENTS[*]

We have previously determined the diffusion length in p-type GaAs:Ge on the basis of photoemission measurements[13]. However, since this type of material constitutes a major element of the cold-cathode structure, we have now performed additional measurements using more direct techniques. In particular, we were interested in determining the diffusion length in highly doped material (10^{19} cm^{-3}). The use of such material is advantageous in reducing the series resistance of the diode and, moreover, in reducing the width of the energy distribution of the emitted electrons (see Fig. 21).

The GaAs epitaxial layers were grown in a boat similar to that previously described[15], from solutions of Ga, As, and Ge. Growth was initiated at 900°C, and, in order to minimize doping gradients in the layers, the solution was cooled only a total of 10°C at a rate of 0.25°C/min. The layers (20 to 30 µm thick) were wiped clean at 890°C by pulling the wafer into a bin adjacent to the one containing the Ga solution.

The samples described here were grown from solutions containing Ga/Ge atomic ratios of 10(#1), 100(#2), and 1000(#3). The substrates were (100) oriented semi-insulating (10^8 Ω-cm) GaAs:Cr or GaAs:Si wafers with an electron concentration of 2 x 10^{18} cm^{-3}. The dislocation density of the latter substrates was <100 cm^{-2}. Hall measurements of the "comparison" samples grown on the semi-insulating substrates yielded the electron concentrations shown in Table IV for samples #1 and #2 which are in good agreement with the values previously reported[16] for material similarly grown. The carrier concentration of sample #3 was determined from C-V measurements of the abrupt p-n junction formed between the epitaxial layer and the substrate. Since material grown from undoped Ga solutions had electron concentrations of about 3 x 10^{16} cm^{-3}, sample #3 was significantly compensated by background impurities.

The diffusion length was directly measured by using two techniques. The first method, using the laser beam scan across a beveled p-n junction, is sensitive to surface recombination since the light is strongly absorbed near the surface. The second technique, using penetrating α-particles, is much less sensitive to the surface condition but is useful under more restrictive conditions.

A. DIFFUSION LENGTH MEASUREMENT USING LASER SCAN

The samples were prepared for laser beam spot scanning by first cleaving bars from the epitaxial wafers on which a Sn-Ni-Au ohmic contact had been applied to the n-type substrate side. The cleaved bars, about 0.5 cm wide and 0.7 cm long, were then lapped at an angle of 1° to the junction along their length. This was followed by a 1% Br-methanol or 5:1:1 sulfuric acid:peroxide: water etch to remove any mechanical damage which may have been introduced.

_____

[*]The work described in this section was performed in collaboration with M. Ettenberg.

TABLE IV

Major Material Parameters and Diffusion Length Values in GaAs:Ge

Sample #	Ga/Ge Atomic Ratio in Solution	$N_A - N_D$ (cm^{-3})	Estimated Electron Mobility (cm^2/V-sec)	Diffusion Coefficient D (a) (cm^2/sec)	Diffusion Length L (b) (μm)	(c) (μm)	Surface Recombination Velocity Sx10^6 (cm/sec)
1	10	1.1×10^{19}	1500	40	5.5	5.6	---
2	100	2.0×10^{18}	3500	90	10.5	11.5	1.1
3	1000	6×10^{16}	6500	165	20.0	16.0	0.74
4	10	1.2×10^{19}	---	---	5.9	---	---

(a) Calculated from estimate of electron mobility.

(b) From laser beam scan measurement.

(c) From α-particle scan measurement.

The angle-lapped bar was then placed on a movable stage, and a point contact was made to the p-type epitaxial layers except for the lowest doped sample, #3, where ohmic contact was made to the p-layer with a bonded Au-Zn wire. The connection to the n-side of the junction was made by a mechanical contact between the stage and the ohmic contact to the substrate. In all cases, the large-area, angle-lapped p-n junction had good diode I-V characteristics.

The 0.5-mW He-Ne laser beam (λ = 6328 Å) was collimated with a 20 X microscope objective and one auxiliary lens. The optical system, using two 10% mirrors, allowed simultaneous visual examination of the collimated laser spot and the angle-lapped surface. The smallest attainable spot size was 12 μm in diameter. A filter (Corning #1-56) was used to ensure that no infrared radiation emanating from the laser impinged on the sample. The entire experimental setup is shown in Fig. 31.

The diffusion lengths were determined by scanning the laser spot along the angle-lapped specimen and measuring the short-circuit current as a function of distance from the p-n junction at intervals of 25 μm. The p-n junction position was accurately determined by noting a maximum in the short-circuit current as a function of position. From an extrapolation of absorption data for GaAs[17] at 6328 Å, the laser light is attenuated by (1/e) in 0.25 μm. The estimated resolution in the diffusion length value is ∿0.5 μm.

The short-circuit current was measured by mechanically chopping the laser beam and using a PAR lock-in amplifier and digital millivoltmeter to determine the voltage across the short-circuiting resistor. Resistors of 1 Ω, 10 Ω, and

46
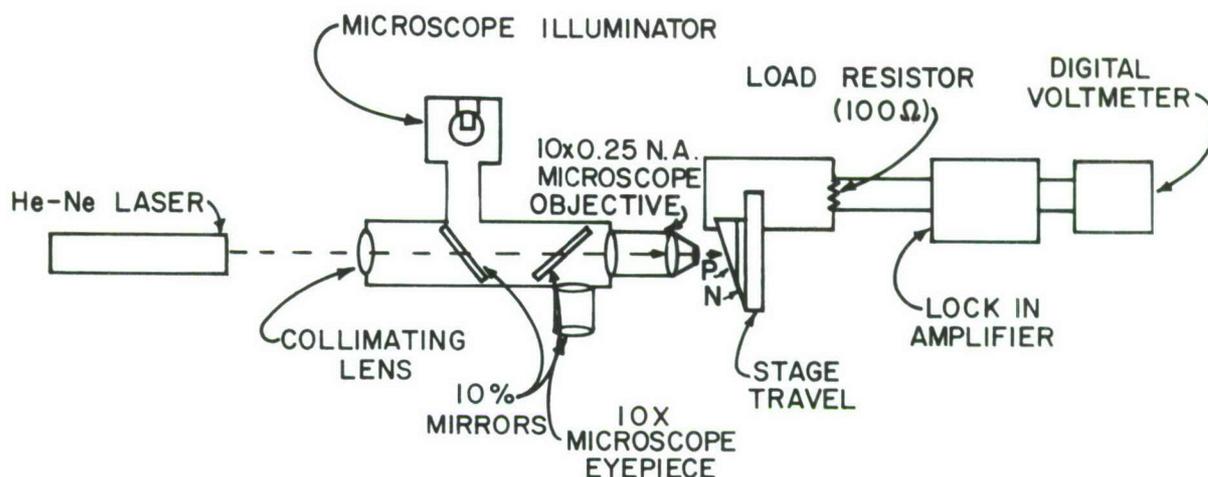
Figure 31. Scanning laser beam method for electron diffusion length measurement.

100 Ω yielded identical results. The 100-Ω resistor was used for maximum signal. The laser beam was also used to determine the angle of the beveled specimen by measuring the angle between the beams reflected from the angle-lapped surface and a plate parallel to the back of the sample. The error in this measurement was not more than 5%. Microscopic examination of etched cleaved edges showed that the p-n junction was parallel to the back of the sample.

The short-circuit current on a relative scale is plotted in Fig. 32 as a function of the p-layer thickness for the specimens studied. The thickness was determined from the measured angle of the beveled surface and the lateral distance from the p-n junction.

The functional relationship between short-circuit current and the p-layer thickness in photodiodes was previously derived[18]. For incident light which does not penetrate into the n-side, the short-circuit current I_{SC} is a function of the surface recombination velocity S, the minority-carrier diffusion coefficient D, the minority-carrier diffusion length L, and the absorption coefficient of the incident radiation ($\sim 10^5 cm^{-1}$ in this case). For $\alpha x > 1.0$, where x is the p-layer thickness and $\alpha > 1/L$, I_{SC} is given by

$$I_{SC} \propto \frac{1}{\left(\frac{S}{D} + \frac{1}{L}\right) e^{x/L} - \left(\frac{S}{D} - \frac{1}{L}\right) e^{-x/L}} \quad (11)$$

or

$$I_{SC} \propto \frac{1}{e^{x/L} - Re^{-x/L}} \quad (12)$$

47
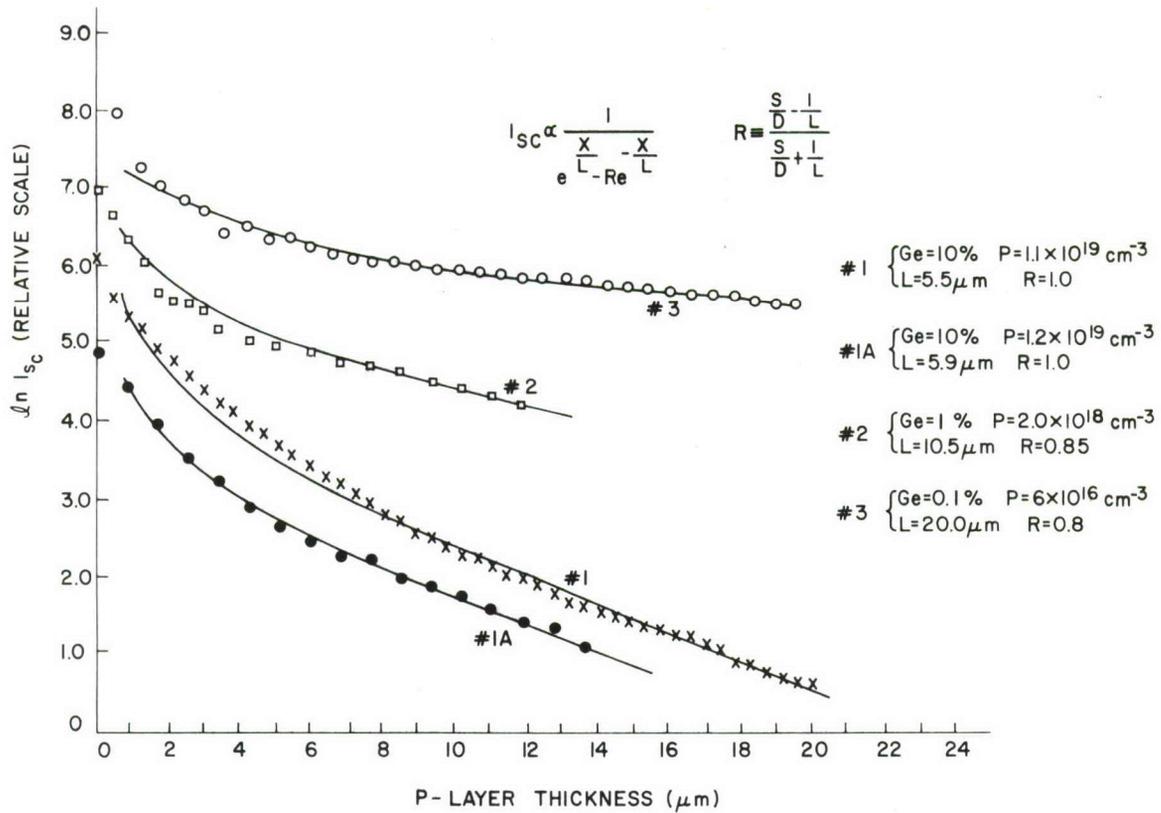
Figure 32. Short-circuit current as a function of the thickness of the p-layer which is illuminated by the laser beam.

where

$$R \equiv \left(\frac{S}{D} - \frac{1}{L}\right) \bigg/ \left(\frac{S}{D} + \frac{1}{L}\right) \tag{13}$$

For $x > L$, the first term in the denominator of Eq. (11) predominates, and the slope of the $\ln (I_{SC})$ vs. x plot yields the diffusion length L directly. The L values obtained for four samples studied are shown in Table IV. The shape of the curve for $x \leq L$ depends on whether S/D is greater or smaller than 1/L. Having estimated L, we can obtain R by fitting Eq. (12) to the data in Fig. 32. The value of R varies between 1.0 and 0.8, depending on the doping level. Values of D may be estimated by assuming that the mobility of electrons in p-type material is the same as that in n-type of the same carrier density. From the experimental value of R and L and the estimated value of D, a value of S ranging from 8 to 11 x 10^5 cm/sec for the etched GaAs surface was derived and is listed in Table IV.

In order to check the reproducibility of the material, two similarly grown 10 Ga:1 Ge samples (#1 and #4) were measured. As shown in Table IV, the L values (5.5 and 5.9 μm) were comparable.

48

B. DIFFUSION LENGTH MEASUREMENT USING α-PARTICLES

Since any measurement technique may contain systematic errors, we checked the diffusion length results with a completely different technique, one developed by Goldstein[19], in which a cleaved p-n junction is scanned with a collimated beam of α-particles 1 μm in diameter. The main advantage of this method is the large depth of α-particle penetration, 15 μm in GaAs, compared with 1.7 μm for 20-keV electrons, and less than 1 μm for photons with greater than bandgap energy. This large α-particle penetration depth eliminates many of the analysis problems associated with surface recombination.

The diodes employed were made from the same material used for the laser scan measurements described earlier. The material was cleaved into bars 450 μm wide and then sawed into diodes 120 μm wide and soldered onto headers.

The 5.3-MeV α-particles were obtained from a (Po)210 source about 50 mCi in strength collimated by a 1-μm hole in a 24-μm-thick metal diaphragm. The distance x from the junction was varied by means of a differential screw thread having 0.2-μm resolution. The charge collected at the junction was measured with a charge storage amplifier and displayed on an oscilloscope.

The charge q collected by the junction is given by

$$q = q_o \exp \left(-\frac{x}{L} \right) \tag{14}$$

where q is the charge produced by the α-particle at a distance x from the junction for a minority-carrier diffusion length L. The charge q is deduced from the maximum height of the envelope of pulses produced by the α-particle beam. The carrier diffusion length L is obtained from the slope of a semilogarithmic plot of the collected charge q as a function of the distance x. The L values thus derived are listed in Table IV and are in very good agreement with those inferred from the laser beam scan method.

REFERENCES

1. The concept of negative electron affinity was first proposed by R. E. Simon in 1963. Experimental realization was by J. J. Scheer and J. van Laar, Solid State Communications 3, 189 (1965).

2. H. Kressel, E. S. Kohn, H. Nelson, J. J. Tietjen, and L. R. Weisberg, Appl. Phys. Letters 16, 359 (1970).

3. G. A. Antypas, L. W. James, and J. J. Uebbing, J. Appl. Phys. 41, 2888 (1970).

4. L. W. James, and J. L. Moll, Phys. Rev. 183, 740 (1969).

5. H. Schade, H. Nelson, and H. Kressel, Appl. Phys. Letters 18, 121 (1971).

6. L. W. James, G. A. Antypas, J. Edgecumbe, R. L. Moon, and R. L. Bell, J. Appl. Phys. 42, 4976 (1971).

7. H. Nelson, U. S. Patent No. 3,565,702.

8. H. Kressel, F. Z. Hawrylo, and N. Almeleh, J. Appl. Phys. 40, 2248 (1969).

9. T. E. Madey and J. T. Yates, J. Vac. Sci. Technol. 8, 525 (1971).

10. See, for example, G. W. Gewartowski, and H. A. Watson, *Principles of Electron Tubes*, (Van Nostrand, Princeton, N. J., 1965) p. 5 ff.

11. D. J. Bartelink, J. L. Moll, and N. I. Meyer, Phys. Rev. 130, 972 (1963).

12. See, for example, Ref. 10, p. 60.

13. H. Schade, H. Nelson, and H. Kressel, Appl. Phys. Letters 18, 121 (1971).

14. L. W. James, G. A. Antypas, J. Edgecumbe, R. L. Moon, and R. L. Bell, J. Appl. Phys. 42, 4976 (1971).

15. H. F. Lockwood and M. Ettenberg, J. Crystal Growth 15, 81 (1972).

16. F. E. Rostoczy, F. Ermanis, I. Hayashi, and B. Schwartz, J. Appl. Phys. 41, 264 (1970).

17. I. Kudman and T. Seidel, J. Appl. Phys. 33, 771 (1962).

18. J. J. Loferski and J. J. Wysocki, RCA Review 22, 38 (1961).

19. B. Goldstein, J. Appl. Phys. 42, 2570 (1971).

DISTRIBUTION LIST

Defense Documentation Center
Attn: DDC-TCA
Cameron Station (Bldg 5)
Alexandria, Virginia   (12)

Naval Communications Command
Attn: COMNAVCOMM(N2)
5827 Columbia Pike
Baileys Crossroads, VA 22041

Commanding General
U.S. Army Materiel Command
Attn: Rsch, Dev & Engr Dir
Washington, DC 20315

Dir of Def Res & Engnrng
Attn: Technical Library
RM 3E-1039 The Pentagon
Washington, D.C. 20301

Rome Air Development Center
EMTLD – Attn: Documents Library
Griffiss AFB, New York 13440

CG, U.S. Army Missile Command
Redstone Scientific Info Center
Attn: Chief, Document Section
Redstone ARsenal, Ala 35809
                                    (3)

Chief of Naval Research
Attn: Code 427
Department of the Navy
Washington, D.C. 20325

Electronic Systems Div (ESTI)
L.G. Hanscom Field
Bedford, Mass 01730
                                    (2)

Commanding General
U.S. Army Weapons Command
Attn: AMSWE-RER-L
Rock Island Illionis 61201

Naval Ships Systems Command
Attn: Code 20526 (Tech Library)
Main Navy Bldg, RM 1528
Washington, DC 20325

Recon Central/AVRS
AF Avionics Laboratory
Wright-Patterson AFB, Ohio 45433

HQ U.S. Army Aviation SYSCOM
Attn: AMSAV-C-AD
P.O. Box 209
St. Louis, MO 63166

Naval Ships Systems Command
Attn: Code 61798
Department of the Navy
Washington, D.C. 20360

U.S. Air Force Security Service
Attn: TSG
San Antonio, Texas 78241

Commanding Officer
Harry Diamond Laboratories
Attn: Library
Washington, D.C. 20438

Director
U.S. Naval Research Lab
Attn: Code 2027
Washington, DC 20390
                                    (2)

HQ, Air Force Systems Command
Attn: SCTSE
Andrews AFB, Maryland 20331

Commanding Officer
U.S. Army Electronic Prvng Grnd
Attn: STEEP-TA-E
Fort Huachuca, Arizona 85613
                                    (2)

Commanding Officer & Director
U.S. Navy Electronics Lab
Attn: Library
San Diego, CA 92152

Air University Library (3T)
Maxwell AFB, Alabama 36112

Commanding Officer
Picatinny Arsenal
Attn: SMUPA-VA6, Bldg 59
Dover, N.J. 07801
                                    (2)

Commander
U.S. Naval Ordnance Lab
Attn: Technical Library
White Oak, Silver Spring
Maryland 20910

Air Force Weapons Laboratory
Attn: WLIL
Kirtland AFB, New Mexico 87117

Commanding Officer
U.S. ARmy Mat'ls & Mech Rsh Cen
Attn: AMXMR-ATL Tech Libry Brch
Watertown, Mass 02172

Air Force Systems Command
STLO (SCTL-16)
Naval Air Development Center
Johnsville,
Warminster, PA 18974

OFC, Asst Sec of Army (R&D)
Attn: Asst for Research
Room 3-E-373 The Pentagon
Washington DC 20310

Commanding Officer
Aberdeen Proving Ground
Attn: Tech Library Bldg 313
Aberdeen Prvng Grnd, MD 21005
                                    (2)

Commandant, Marine Corps
HQ U.S. Marine Corps
Attn: Code A04C
Washington, DC 20380

Chief, Research & Development
Department of the Army
Washington, D.C. 20315
                                    (2)

Commanding Officer
U.S. Army Limited War Lab
Aberdeen Prvng Grnd, MD 21005

Marine Corps Dev & Educ Cmd
Development Cen, Attn: C-E Div
Quantico, Virginia 22134

Commanding General
U.S. Army Materiel Command
Attn: AMCMA-FE
Washington, DC 20315

Commanding Officer
U.S. Army Garrison
Attn: Tech Ref Div
Fort Huachuca, Arizona 85613

Commander
U.S. Army Research Office
Box CM- Duke Station
Durham, North Carolina 27706

Commanding Officer
U.S. Army Mobility Equp R&D Cntr
Attn: Tech Document Cen Bldg 315
Fort Belvoir, VA 22060
(2)

Commanding Officer
U.S. Army Engineer Topo Labs
Attn: ETL-TE
Ft. Belvoir, VA 22060

U.S.Army Sec Agcy Combat Dev Act
Attn: IACDA-P(T) & 1ACDA-P(L)
Arlington Hall Station Bldg 420
Arlington VA 22212
(2)

U.S. Army Sec Agcy Proc Ctr
Attn: IAVAPC-R&D
Vint Hill Farms Station
Warrenton, VA 22186

Commandant
U.S. Army Air Defense School
Attn: C&S Dept, MSL Sci Div
Fort Bliss, Texas 79916

Director
U.S. Army Advanced Matl Concpts
Attn: AMXAM
Washington, D.C. 20315

Commanding Officer
U.S. Army Combat Dev Command
Communications-Electronics Agcy
Ft. Monmouth, N.J. 07703

Commanding General
U.S. Army Satellite Comm Agcy
Attn: Tech Doc Cntr
Ft. Monmouth, N.J. 07703

U.S. ArmyLiaison Office
MIT, Bldg 26, RM 131
77 Massachusetts Avenue
Cambridge, Mass 02139

U.S. Army Liaison Office
MIT-Lincoln Lab, Rm A210
P.O. Box 73
Lexington, Mass 02173

Headquarters
U.S. Army Combat Dev Command
Attn: CDCLN-EL
Ft. Belvoir, VA 22060

Commanding General
U.S. Army Tank-Automotive Cmnd
Attn: AMSTA-Z, R. McGregor
Warren, Michigan 48090

USAECOM Liaison UFC, Stanfd Univ
Solid State Electronics Lab
McCullough Bldg
Stanford, CA 94305

Chief
Missile Electronic Warfare
EW Lab, USA Electronics Cmnd
White Sands Missile Range,
New Mexico 88002

Commanding General
U.S. Army Electronics Cmnd
Ft. Monmouth, N.J. 07703

Attn: AMSEL-TE

Commanding General
U.S. Army Electronics Cmnd
Ft. Monmouth, N.J. 07703

Attn: AMSEL-ME-NMP-PS

Commanding General
U.S. Army Electronics Comnd
Ft. Monmouth, N.J. 07703

Attn: AMSEL-TD-TI   (2)

Commanding General
U.S. Army Electronics Command
Ft. Monmouth, N.J. 07703

Attn: AMSEL-RD-MT

Commanding General
U.S. Army Electronics Command
Ft. Monmouth, N.J. 07703

Attn: AMSEL-RD-LNS

Commanding General
U.S. Army Electronics Command
Ft. Monmouth, N.J. 07703

Attn: AMSEL-XL-D

Commanding General
U.S. Army Electronics Command
Ft. Monmouth, N.J. 07703
Attn: AMSEL-NL-D

Commanding General
U.S. Army Electronics Command
Ft. Monmouth, N.J. 07703

Attn: AMSEL-WL-D

Commanding General
U.S. Army Electronics Command
Ft. Monmouth, N.J. 07703

Attn: AMSEL-VL-D

Commanding General
U.S. Army Electronics Command
Ft. Monmouth, N.J. 07703

Attn: AMSEL-HL-CT-D   (3)

Commanding General
U.S. Army Electronics Command
Ft. Monmouth, N.J. 07703

Attn: AMSEL-BL-D

Commanding General
U.S. Army Electronics Command
Ft. Monmouth, N.J. 07703

Attn: AMSEL-KL-DT

Commanding General
U.S. Army Electronics Command
Ft. Monmouth, N.J. 07703

Attn: AMSEL-KL-TQ   (3)

Commanding General
U.S. Army Electronics Command
Ft. Monmouth, N.J. 07703

Attn: AMSEL-TL-BA

Director, Electronic Def Labs
Sylvania El-ctric, Inc
Attn: Doc ACQ Library
P.O. 205
Mountain View, CA 94040

NASA Scientific & Tech Info Fac
Attn: Acquisitions Branch
(S-AK/DL)
P.O. Box 33
College Park, MD 20740   (2)

Project SETE
NYU College of Engnrng & Science
401 W. 205th St (Rsch Bldg 2)
New York, N.Y. o0034

Advisory Group on Electron Devic
201 Varick St, 9th Flr
New York, N.Y. d0014
(2)

Battelle Defender Info Cntr
Battelle Memorial Institute
505 King Ave
Columbus, Ohio 43201

Remote Area Conflict Info Cntr
Battelle Memorial Institute
505 King Avenue
Columbus, Ohio 43201

Defense Ceramic Info Cntr
Battelle MEmorial Institute
505 King Avenue
Columbus, Ohio 43201

Strategic Technology Office
Information Analysis Cntr
Battelle Memorial Institute
505 King Avenue
Columbus, Ohio 43201

Defense Metals Info Cntr
Battelle Memorial Institute
505 King Ave
Columbus, Ohio 43201

Stanford Research Institute
Menlo Park, CA 94025
Attn: Louis Heynick

Plastics Tech Eval Cntr
Picatinny Ars,Bldg 3401
Dover, N.J. 07801

Corning Glass Works
3800 Electronics Drive
Raleigh, N.C.

Attn: Marian Goodman

Radiation Eff Info Cntr
Battelle Memorial Institute
505 King Avenue
Columbus, Ohio 43201

Lawrence Radiation Lab
Technical Info Dept L-3
P.O. Box 808
Livermore, CA 94550

Reliability Analysis Cntr
Rome Air Dev Cntr
Attn: AMERR
Griffiss AFB, N.Y. 13440

Commanding General
USACDC Intell & Control SysGrp
Ft. Belvoir, VA 22060

Shock & Vibration Info Cntr
Naval Research Lab Code 6020
Washington, DC 20390

Commanding General
U.S. Army Combat Dev Command
Attn: CDCMS-E
Ft. Belvoir, VA 22060

Thermophysical Props Res Cntr
Purdue Univ, Research Park
2595 Yeager Rd
Lafayette, Indiana 47906

Commanding General
USACDC Prsnl & Log Sys Grp
Attn:CDCPALS-MA
Ft. Lee, VA 23801

VFLA Seismic Info Center
U of Michigan
Box 618
Ann Arbor, Michigan 48107
(3)

Commanding General
USACDC Combat Sys Trp
Attn; CDCCOMSS-SS
Ft. Leavenworth, Kansas 66027

Commanding General
U.S. Army Materiel Command
Attn: AMCRD-R H. Cohen
Washington DC 20315

Commanding Officer
USACDC Nuclear Agency
Ft. bliss, Texas 79916

Director
Advanced Research Projects Agcy
Washington, D.C. 20301
Attn: Progrm Management
(3)

Commanding Officer
USACDC Special Operations Agy
Ft. Bragg, N.C. 28307

DOCUMENT CONTROL DATA - R & D	
(Security classification of title, body of abstract and indexing annotation must be entered when the overall report is classified)	

1. ORIGINATING ACTIVITY *(Corporate author)*

RCA Laboratories
Princeton, New Jersey   08540

2a. REPORT SECURITY CLASSIFICATION

Unclassified

2b. GROUP

N/A

3. REPORT TITLE

OPTOELECTRONIC ELECTRON EMITTER

4. DESCRIPTIVE NOTES *(Type of report and inclusive dates)*

Final Report   15 October 1970 to 31 December 1972

5. AUTHOR(S) *(First name, middle initial, last name)*

Horst E. P. Schade, Herbert Nelson, Henry Kressel, and Wieslaw W. Siekanowicz

6. REPORT DATE

May 1973

7a. TOTAL NO. OF PAGES

66

7b. NO. OF REFS

19

8a. CONTRACT OR GRANT NO.

DAAB07-71-C-0059

b. PROJECT NO.

79   1021   7034401

c. ARPA Order No. 1686

d.

9a. ORIGINATOR'S REPORT NUMBER(S)

PRRL-73-CR-11

9b. OTHER REPORT NO(S) *(Any other numbers that may be assigned this report)*

ECOM-0059-F

10. DISTRIBUTION STATEMENT

Approved for public release; distribution unlimited.

11. SUPPLEMENTARY NOTES

12. SPONSORING MILITARY ACTIVITY

United States Army Electronics Command
Fort Monmouth, N.J.   07703
AMSEL-TL-BA

13. ABSTRACT Greatly improved cold-cathode structures based on negative-electron-affinity surfaces and on GaAs-(AlGa)As heterojunction structures grown by liquid phase epitaxy were developed. Emission efficiencies (emission current/junction current) were 35 times better than at the start of our research. Pulsed emission current (I_e) densities were as high as 7 A/cm^2 (1.7 mA total I_e), the highest yet reported for III-V compound semiconductor cold-cathodes based on negative-electron-affinity surfaces. Reproducible dc operation was obtained with efficiency as high as 1.9%, and I_e and current densities up to 190 µA and 0.4 A/cm^2, respectively. A key property of the semiconductor cold-cathode, the half-width of the energy distribution of electrons emitted from a GaAs-(AlGa)As structure, was found to be 160 meV, distinctly narrower than that for a conventional thermionic cathode. No significant difference in cathode performance was found in studies of dc operation and cathode life under continuously pumped vacuum conditions and in sealed tubes. Operation was obtained for a period of 360 hr. Shelf-life of cathode efficiency in sealed tubes was essentially constant up to 5 months. A major source for rapid degradation of emission efficiency is electron-stimulated desorption from the collector electrode; methods to reduce such degradation are given. Finally, optoelectronic cold-cathodes were incorporated into electron-beam-injected transistor (EBIT) tubes. The activation procedures of the cathode did not adversely affect the performance of the EBIT targets. Their reverse I-V characteristics did not degrade, and the current gains ($\approx$1200 at 9 kV) and threshold beam voltages were virtually identical to those from conventional oxide and thoria cathodes. Advantages of the semiconductor cold cathodes are: instantaneous operation, simple pulsed operation, lower noise, and lower power requirements.

DD FORM 1 NOV 65 **1473**

14. KEY WORDS	LINK A		LINK B		LINK C	
	ROLE	WT	ROLE	WT	ROLE	WT
Electron Emission						
Electron Emitters						
Semiconductor Cold-Cathodes						
Semiconductor Cold-Cathode Structures						
Negative Electron Affinity						
Low Work Function						
GaAs						
(AlGa)As						